J. Fluid Mech. (1986), *vol.* 171, *pp.* 219–261
Printed in Great Britain

Boundary-layer receptivity to unsteady pressure gradients: experiments and overview

By M. NISHIOKA

College of Engineering, University of Osaka Prefecture, Sakai, Osaka, Japan

AND M. V. MORKOVIN

Department of Mechanical and Aerospace Engineering, Illinois Institute of Technology, Chicago, IL 60616, U.S.A.

(Received 11 September 1984 and in revised form 2 April 1986)

The experimental evidence on the mechanisms of forcing of unstable vorticity waves (the Tollmien–Schlichting–Schubauer or TS waves) of circular frequency ω and wavelength λ_{TS} in wall layers by unsteady pressure gradients of amplitude A and frequency ω is reviewed and found to be confused and contradictory. It is proposed that a likely effective receptivity mechanism rests on the fact that under realistic conditions A varies with distance x along any body of finite thickness, $A(x)$, and introduces thereby additional characteristic lengths which can match λ_{TS}. Heuristic arguments suggest that through $A(x)$ the pressure gradient infuses vorticity at the wall and forces spatial growth of the TS mean-square vorticity $\overline{\zeta^2}$, at a rate proportional to the real part of $\Delta A_F(k_{TS})$, the contribution of $A(x)$ between $x-\frac{1}{2}\lambda_{TS}$ and $x+\frac{1}{2}\lambda_{TS}$ to the Fourier transform $A_F(k)$ at $k = k_{TS}$. A second input into $\overline{\zeta^2_{TS}}$ growth corresponds to the conversion of the steady boundary-layer vorticity into unsteady ζ_{TS}, through the action of v_f, the normal velocity of the forcing field. The rate is given by $\int_0^\delta \overline{v_f \zeta_{TS}}\, U''(y)\,dy$ and is proportional to the imaginary part of $k_{TS}\Delta A_F(k_{TS})$.

The proposition is consistent in all currently verifiable respects with one numerical and a series of laboratory experiments. In the laboratory experiments, various configurations of a pulsating pressure source and shielding plates located in the free stream supplied the variable-amplitude pressure gradients over the nearby flat-wall boundary layer. Three of the cases presented here demonstrate that stationary unsteady pressure fields induce Stokes-like sublayers when the boundary layer is stable and self-excited vorticity waves when it is unstable. The results of a fourth experiment suggest that unsteady pressure sources in wakes near the boundary layer can force the growth of unstable wall waves at the wake frequencies even though their propagation speeds differ. Material is also presented on key Soviet experiments and views on receptivity. Finally, these experiments and ours are examined for consistency and complementarity.

1. Introduction

Ever since the 1943 experiments of Schubauer & Skramstad (1948) it has been generally accepted that propagating shear-wave solutions of the Orr–Sommerfeld (OS) equations can be generated by 'external oscillating fields' which are fixed, i.e. 'standing' with respect to a laboratory observer. Both their vibrating ribbon and their oscillating pressure field issuing through a small hole in the wall under the

Blasius boundary layer set up forced local standing fields of the form $V_{nf} = f_{nf}(x, y, z) \exp(-i\omega t)$; here f_{nf} represents the velocity vector, and the subscript f indicates forcing. At downstream distances, sufficiently long for the particular solution of the forced system to decay to negligible values, the observed response of their boundary layer was experimentally indistinguishable from free solutions of the homogeneous Orr–Sommerfeld equations as then known.

Gaster's concepts of spatially developing instability waves make a conceptualization of the Schubauer–Skramstad experiments quite straightforward. At some station x_i, slightly downstream from the ribbon or the hole, the measurable unsteady fields $f_n(x_i, y, z) \exp(-i\omega t)$ constitute initial conditions at the plane x_i = constant for the spatial development of the long-range linearized response of the boundary layer. According to Salwen & Grosch (1981), the initial fields (at least in the two-dimensional case of the ribbon) can be represented in terms of the discrete and continuous spectral y-eigenfunctions of the OS solutions associated with the forcing frequency ω. The contributions from the discrete spectra, other than the fundamental, decay rapidly downstream, and the response field should then evolve into the characteristic Tollmien–Schlichting–Schubauer (TS) travelling waves observed by Schubauer & Skramstad. In this linear system, of course, the initial conditions in time become irrelevant after the more complex vorticity fields generated at the start of the oscillations are convected off the plate. Gaster (1975) and Gaster & Grant (1975) successfully extended these concepts to the spatio–temporally evolving wave packets in the (x, z)-plane when the boundary layer was disturbed by an impulse-like puff from a hole under the layer.

These classical experiments in which the forcing disturbances were introduced very *locally* within the boundary layer are now recognized as special cases of receptivity of shear layers to externally imposed disturbance fields, either standing or propagating with speeds distinctly different from those of the free OS solutions. For further clarification, the reader is referred to Reshotko's (1976) discussion of receptivity and its relation to the onset of turbulence in the boundary layer caused by the presence of weak turbulent and acoustic fluctuations in the free stream. The early experimental evidence for receptivity mechanisms was outlined by Morkovin (1978, pp. 12–15).

Experiments on the receptivity to unsteady pressure fields including sound have been particularly inconclusive, if not confusing. With a few exceptions, they suffered from (i) poor quantitative characterization of the forcing field along the outer edge of the boundary layer, (ii) inadequate local information on the fluctuations in the boundary layer in the region where the stimulated unstable response starts growing, (iii) lack of documentation of potentially singular diffraction fields around the leading edge and/or the singular effects of vibrations of the leading edge, and (iv) excessive forcing disturbance levels. Therefore only the more revealing, less speculative references are discussed here. Improving on (i) and (ii) is necessary if the several possible mechanisms of receptivity are to be reliably identified. Removing deficiencies of type (iii) and (iv) would eliminate many of the current speculations about secondary receptivity paths in past experiments.

To be sure, experiments on receptivity to unsteady pressure gradients are very difficult; desiderata are more easily formulated than they are satisfied in practice. Because of their non-parabolic nature, ambient pressure fields generally influence the whole flow field and are not restricted to local boundary-layer effects as in the Schubauer–Skramstad experiments. Furthermore, wakes from any support systems including probes are much more sensitive to sound than wall boundary layers; near wakes can become secondary sources of unsteady pressure fields which may

contaminate the primary forcing field. Because of the pervasive nature of the forcing pressure fields, any local measurement of the fluctuating x-component of perturbation velocity $|u| \exp(-i\omega t + i\phi_u)$ represents a superposition of the primary and secondary forcing fields, as well as the evolving standing and propagating response fields. At present there is no operational way of decomposing the signal into its constituent fields. To aid the decomposition in two-dimensional experiments the actual periodic forcing pressure fields are best specified by measuring $|u|$ and ϕ_u along a contour surrounding the (x, y)-region where the conversion to TS vorticity waves takes place, or by equivalent 'input' measurements.

With the exception of the Morkovin–Paranjape (1971) study of acoustic forcing of two-dimensional jets and shear layers, in past experiments sound was beamed at the models 'globally', from rather remote fixed loudspeakers at high sound levels of 95–120 dB. The fixed sound-model geometries made comparisons among experiments more difficult. The high disturbance levels can evoke response through nonlinear mechanisms, leading to receptivity paths and transition through higher harmonics, as observed by Knappe & Roache (1966, figure 34) and Vlasov, Ginevskii & Karavosov (1977, figure 5). High sound levels also tend to bring local acoustic resonances to non-negligible levels (e.g. Shapiro's 1977, figure 11, contaminating standing waves) and to structural resonances. In fact, Kachanov, Kozlov & Levchenko (1975) found a convincing correlation between the vibrations of their 1 cm thick flat plate as function of the frequency of forcing acoustic fluctuation and the observed instability growth and transition: they point to the acoustically induced vibrations of the leading edge as the probable dominant cause of their transition.

In the same wind tunnel, an imaginative use of two travelling sensors by Polyakov, Domaratskii & Skurlatov (1976) disclosed two types of responses on their sturdier 2.5 cm thick plate. In one response, rapid growth of unstable propagating shear waves was observed to 'start' at conditions corresponding to a locus halfway between the two branches of the theoretical neutral curve, their figure 7. In a second response (their figure 5), fluctuations in the boundary layer existed at the upstream reach of their traversing probe, decayed somewhat and then started growing again near the same locus as the first group. Both groups reached maximum amplitude at the upper branch of the neutral curve and could be observed for some distance into the damped region (their figure 7). Originally Polyakov *et al.* stated that the second group of early excited waves remained unexplained, but in 1979 after lengthy discussion Polyakov agreed with Kachanov *et al.* (1975) that it probably represented waves excited near the leading edge by vibrational motion or some other singular behaviour. These are typical speculations consistent with the available but very inadequate database. Other speculations on the behaviour of the fluctuations in the flat-plate experiments by Shapiro (1977) were advanced by Leehey & Shapiro (1980) and Leehey (1980). To support Leehey's speculations, Gedney (1983) demonstrated that TS waves excited by a loudspeaker on the same 1.25 cm thin plate with a 6:1 semi-elliptic nose, could be effectively cancelled by vibrating the plate leading edge with the right phase and amplitude. We shall return to the issue of leading-edge vibrations in §§5.2 and 5.3.

The interest of Soviet experimentalists in receptivity to moving external vortex flows and to acoustic environments led to many papers published in Russian from about 1967. The more important results have been summarized in two Russian monographs, Ginevskii, Vlasov & Kolesnikov (1978) and, especially, Kachanov, Kozlov & Levchenko (1982, pp. 7–44, 135–139), hereinafter referred to as KKL (1982). KKL (1982) present their interpretation of the experimental receptivity

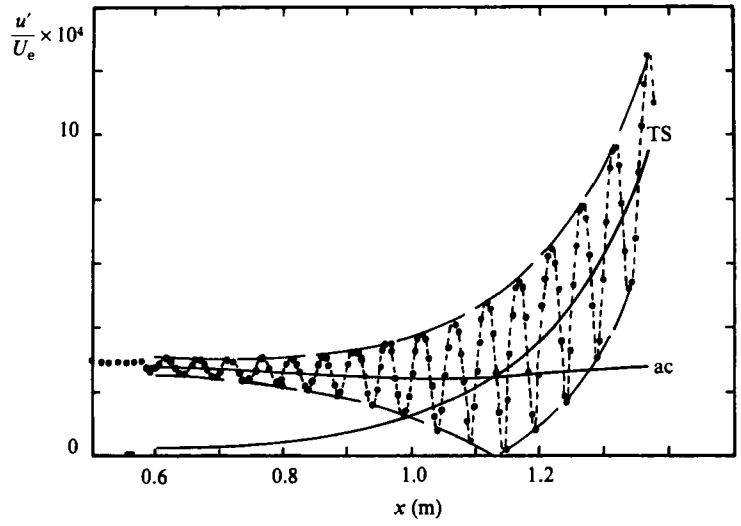

FIGURE 1. Hot-wire measurements of total signal u' yielding an interference pattern between a forcing acoustic wave of 138 Hz at nearly constant 104 dB and the growing TS response on a flat plate downstream of a strip of Mylar tape 12 mm wide and 34.5 ± 2.5 μm high. As indicated, the tape is 0.565 m from the leading edge at a local Re_{δ^*} of 1550 and $\delta^* \approx 1$ mm. Aizin & Polyakov (1979).

paths on pp. 40–44. Unfortunately, the experience and views on receptivity of the Novosibirsk school remain virtually unknown outside the USSR; their essence is described in §5 where we search for a broader view which would accommodate all the reliable experiments. The KKL brief reference to Aizin & Polyakov (1979), an unpublished paper in Russian, received after the first draft of this paper, deserves amplification; see the Appendix. Their key graph represents the clearest illustration of receptivity to sound and is reproduced here in figure 1 for conceptual reference. It displays the amplitude of the total horizontal velocity fluctuations at an unspecified height of a flat-plate boundary layer downstream of an extremely thin narrow strip of Mylar fastened to the wall as indicated. (See discussion of equation (3.1) and figure 4 for interpretation.) As the width of the strip is only a quarter of the induced TS wavelength, $\frac{1}{4}\lambda_{TS}$, the region of high receptivity in this case is uncommonly localized. The localized solution of the non-homogeneous problem evidently evolves rapidly into an interference pattern between the upstream-propagating acoustic field and the spatially growing TS wave – the non-decaying part of the solution of the homogeneous problem. This better sample of past investigations makes it clear that identification of the 'start' of the TS response in experiments – e.g. those of Polyakov *et al.* (1976) – is marred by lack of information on the forcing and response fields as functions of x and y. To reveal the nature of the receptivity mechanism numerous detailed profiles of the evolution of the amplitude $u'(x, y)$ and the phase $\phi(x, y)$ in the proximity of the Mylar strip, $0.5 < x < 0.6$ are needed.

In more general situations (as in our experiments) the locally generated vorticity waves will not be perfectly in phase with vorticity waves generated farther downstream, and we should expect less regular early growth, including partial cancellations. In fact, in a layer of constant thickness δ disturbed by an unsteady pressure gradient $\partial p/\partial x$ of *constant* amplitude A, the induced TS waves should cancel as a consequence of the mismatch of the two wavelengths, λ_{TS} and λ_{ac}, at the same frequency. It is

not surprising, therefore, that the TS receptivity of the idealized Blasius boundary layer on a rigid, smooth semi-infinite flat plate to a grazing sound wave is exceedingly small and that its active region should be traceable to the region near the leading edge where x-dependence of the combined system is largest. Analyses of Goldstein (1983) and Goldstein, Sockol & Sanz (1983) as well as numerical calculations of Murdock (1980) imply that the vorticity waves generated in this region would decay by at least three orders of magnitude before they could start amplifying past their critical Reynolds number. The receptivities found by Kachanov *et al.* (1975), Polyakov *et al.* (1976) and Shapiro (1977) on their flat plates with finite thickness are therefore unlikely to rest on the mechanism of Goldstein's (1983) analysis for the evidently over-idealized problem. The most likely cause for enhanced receptivity is sharper dependence on x of the characteristics of the boundary layer and/or of the exciting sound; the cancellation of effects discussed above will then diminish and a measurable TS wave might be able to grow. The x-dependence of the system can arise in many ways; thus a number of receptivity paths can be expected even in the purely linear phenomena; see Goldstein (1985).

In §2 we describe a receptivity mechanism for the general case of flows around bodies with finite thickness in which the amplitude of the unsteady pressure gradient $A(x)$ varies along the surface. The x-dependent growth of the boundary layer is secondary to the mechanism and can be neglected. Also the characteristic lengths induced by *mean* pressure gradients are purposely avoided so as to provide a clear test within the well-known stability characteristics of the Blasius boundary layer. The disturbance velocity field is made up of the periodic forcing field u_f (particular solution of the linearized Navier–Stokes equations), u_{TS} the fundamental-mode field (part of the homogeneous solution), and u_d, the always damped part of the homogeneous solution (made up of higher discrete modes and continuous modes). Heuristic considerations of unsteady vortical fields $\zeta(x, y, t)$ show that time mean square of TS enstrophy $\overline{\zeta_{TS}^2}(x, y)$ is generated at the wall with source strength $\overline{2(\partial p/\partial x)\zeta_{TS}}$ per unit area, and inside the layer at the rate $2U''\overline{v\zeta_{TS}}$ per unit volume as transfer from mean flow vorticity. The net input rate is found to be proportional to a local Fourier transform of $A(x)$, $\Delta A_F(k_{TS})$, evaluated at the wavenumber of the TS field for the given frequency and Reynolds number. In other words, the sole x-variation present, that of the amplitude of $\partial p/\partial x$, $A(x)$, introduces the needed characteristic lengths in the forcing field (besides the acoustic wavelength) which can match the TS wavelength and thereby feed the u_{TS} field.

In §3 we describe the experimental setting, equipment, and techniques designed to mitigate the difficulties (i)–(iv) of earlier experiments on receptivity. The results are presented and discussed in §4. In §5 we attempt to reconcile the experience and views of the Novosibirsk group with ours. Their key work on the role of the leading edge, vibrations due to acoustic loads, and the normal velocity component is briefly described. These and other Soviet experiments and ours are then examined for consistency and complementarity. Appendix 1 contains more detailed information on the paper of Aizin & Polyakov (1979).

2. A receptivity mechanism and its experimental implications

2.1. *Behaviour of unsteady fields near walls*

Since acoustic fields are irrotational except near solid boundaries, it is logical to look to the viscous ('acoustic') sublayers of these pressure fields for one component of mechanisms that could generate the growing vorticity waves. According to the no-slip

boundary conditions, *all* non-uniform pressure fields do generate spanwise wall vorticity sources of strength

$$-\nu\frac{\partial\zeta}{\partial y}=+\nu\frac{\partial^2 u}{\partial y^2}=\frac{1}{\rho}\frac{\partial p}{\partial x},\quad y=0 \tag{2.1}$$

per unit area per unit time, Lighthill (1963, p. 54). Here u is the streamwise velocity component, ν denotes the kinematic viscosity, and p and ρ the pressure and density respectively.

Equation (2.1) applies to both steady and unsteady pressure fields, including acoustic near and far fields. This conversion of unsteady pressure gradients into wall sources of unsteady vorticity is operative in all receptivity paths. Conditions for its positive contribution to growing $\overline{\zeta_{\mathrm{TS}}^2}$ in a strictly parallel Blasius layer are explored in §2.4. For harmonic excitation, the terms in (2.1) represent amplitude and phase relationships after factorization of $\exp(-\mathrm{i}\omega t)$, with ω equal to 2π times the frequency f in Hz. According to Morse & Ingard (1968, p. 289), the solution for a uniform monochromatic wave with acoustic pressure gradient of amplitude A, travelling along a flat plate, and for its viscous sublayer, is to the first order in the small quantity $S=(2\nu/\omega)^{\frac{1}{2}}$, the Stokes thickness,

$$p_{\mathrm{ac}}=\frac{A}{k}\exp \mathrm{i}k(x-ct), \tag{2.2a}$$

$$u_{\mathrm{ac}}=\frac{A}{\rho\omega}\left\{1-\exp\frac{(\mathrm{i}-1)y}{S}\right\}\exp \mathrm{i}k(x-ct), \tag{2.2b}$$

where k represents the wavenumber, and c the speed of sound, so that $\omega=kc$. For $y/S>6$ the field (2.2) becomes operationally indistinguishable from that of the acoustic plane wave $u=p/\rho c$. The associated, outward-diffusing vorticity distribution is large, of order $1/S$:

$$\zeta=\frac{A}{\rho\omega}\frac{\mathrm{i}-1}{S}\exp\frac{(\mathrm{i}-1)y}{S}\exp \mathrm{i}(kx-\omega t). \tag{2.3}$$

Its amplitude decays exponentially away from a high maximum at the wall, where it is fed by the pressure-induced sources in accordance with (2.1). When the acoustic wave is not grazing the wall, the field p_{ac}, u_{ac}, v_{ac} is modified by the reflected wave, but the sublayer terms involving S retain their functional form, Morse & Ingard (1968, p. 289). For infinite wavelength, $k\to 0$, the vorticity distribution is identical with that of an infinite plate oscillating with respect to the fluid at rest, as first derived by Stokes. Theoretical and experimental evidence, summarized by Loehrke, Morkovin & Fejer (1975), indicates that when a mean external flow U is present, (2.2b) and (2.3) with $k\to 0$ are essentially superposable on the mean-flow boundary layer when S is small.

Lin (1955, equation 4.5.7) showed that the distribution (2.3) also fits the near-wall vorticity field in the Tollmien–Schlichting–Schubauer instability waves within boundary layers, provided that c stands for the propagation speed $c=f\lambda_{\mathrm{TS}}=\omega/k_{\mathrm{r}}$ of these waves. For spatially developing TS waves, $k=k_{\mathrm{r}}+\mathrm{i}k_{\mathrm{i}}$; the exponential terms in (2.2b) and (2.3) then stand for $\exp(-k_{\mathrm{i}}x)\exp \mathrm{i}k_{\mathrm{r}}(x-ct)$. The wavelength λ_{TS} of amplified TS waves is on the order of at least 30 displacement thicknesses δ^*, i.e. very much shorter than the acoustic wavelength λ_{ac} at the same frequency. As noted, it is this discrepancy between the characteristic lengths λ_{TS} and λ_{ac} that makes the initiation of TS waves by sound waves a very difficult problem. An acoustically induced Stokes-layer patch of, say, positive vorticity over a half cycle of the sound wave would have to enhance the net amplitude of a large number of

plus–minus vorticity half-cycles of the TS waves. (This will be tested through (2.6) below.)

Actually the wavelength λ_{ac} is the sole characteristic length of the vorticity induced at the wall *only* in the idealized case of a uniform sound beam parallel to the perfectly flat plate of zero thickness. For practical geometries the amplitude A of the forcing waves varies with distance along any shaped body; additional characteristic lengths then arise through the variation $A(x)$, rather than through the harmonic variation in $\exp ikx$ in (2.2*a*). Thus in the experiments of Kegelman & Mueller (1986) reflection and diffraction of the exciting sound fields around the shoulder of an ogive-cylinder model brought forth local variations in $\partial p/\partial x$ on scales much shorter than λ_{ac} and a remarkable sensitivity to excitation over a wide sound frequency range, 500–1000 Hz, at a fixed body Reynolds number of 8×10^5; see dramatic photographs in their figures 8 and 9. If, for a given forcing frequency, the local integration range from $x-\frac{1}{2}\lambda_{TS}$ to $x+\frac{1}{2}\lambda_{TS}$ in the Fourier transform of $A(x)$ yields a substantial contribution in the wavenumbers k_{TSr} amplified in the Tollmien mechanism at that frequency, the amplifiable vorticity waves are among those seeded locally at the wall by $\partial p/\partial x$.

2.2. *Input into periodic vorticity fields*

It is useful to examine the general, complementary linearized differential equations for vorticity and pressure in quasi-parallel incompressible flows for clues on possible evolution of these waves in x and y:

$$\left(\frac{\partial}{\partial t}+U\frac{\partial}{\partial x}\right)\zeta = +vU''+\nu\nabla^2\zeta, \tag{2.4}$$

$$\nabla^2 p = -2\rho U'\frac{\partial v}{\partial x}. \tag{2.5}$$

Here primes denote derivatives with respect to y of the local mean velocity profile $U(y)$. The term $+vU''$ in (2.4) constitutes a source of *unsteady* disturbance vorticity within the boundary layer – a rate of transfer from the *steady* vorticity of the mean flow. Similarly $-2\rho U'\partial v/\partial x$ is a source of the inertial near-field pressure fluctuations characteristic of the low-speed TS waves. In (2.4) the Laplacean of ζ, multiplied by ν, represents the vorticity loss per unit time of an element of unit volume along its path by diffusive smoothing of the local highs and lows of the instantaneous ζ-distributions. These equations also apply locally in the appropriate long-wave limit to the acoustic sublayer and hence to its linear interaction with TS waves.

Since $\partial v/\partial x = ikv$ in harmonically varying flows, both sources above are governed by the y-distribution of the normal velocity v in the waves. It is significant that the v-component in the acoustic sublayer and in any Stokes layer is of higher order. The growth of the TS waves must therefore entail a build-up of v from the wall. We recall that the no-slip conditions impose a slower, parabolic growth $v = \zeta_0 k\{\frac{1}{2}iy^2-(1+i)y^3/6S\}$ near a flat wall (Lin 1955, p. 62). This follows from (2.2*b*), (2.3) and the continuity equation.

An idea of the vorticity growth in x and y can be obtained by multiplying (2.4) by ζ, averaging in time over one period and integrating from the wall to any desired level y:

$$\int_0^y U\frac{\partial\overline{\zeta^2}}{\partial x}\,dy = 2\int_0^y \overline{\zeta v}\,U''\,dy+\nu\int_0^y\frac{\partial^2\overline{\zeta^2}}{\partial x^2}\,dy$$
$$-2\nu\int_0^y\overline{\left(\frac{\partial\zeta}{\partial x}\right)^2}\,dy-2\nu\int_0^y\overline{\left(\frac{\partial\zeta}{\partial y}\right)^2}\,dy+\nu\frac{\partial\overline{\zeta^2}}{\partial y}+\frac{2}{\rho}\overline{\left(\zeta\frac{\partial p}{\partial x}\right)}_0. \tag{2.6}$$

We note that for spatially developing waves the averaging is simplified by using the expression $\mathrm{Re}\{fg^* \exp \mathrm{i}(k_{rf}-k_{rg})x\} \exp\{-(k_{if}+k_{ig})x\}/2$ for the time average of the product of two functions $f(x,y) \exp \mathrm{i}(k_f x-\omega t)$ and $g(x,y) \exp \mathrm{i}(k_g x-\omega t)$; here the asterisks indicate complex-conjugates. Thus $\overline{\zeta^2} = \zeta_0 \zeta_0^* \exp(-2y/S)$ for the non-growing Stokes distribution of equation (2.3). The last term in (2.6) represents the source of $\overline{\zeta^2}$ diffusing out of the wall in accordance with equation (2.1). Together with the preceding term, it gives the net diffusion rate into the slab of height y, which is of order $\overline{\zeta_0^2}\omega y$. These last two expressions balance exactly the fourth term on the right and dominate the entrophy distribution $\overline{\zeta^2}$ near the wall, as expected from the pure Stokes-layer limit behaviour. The effect of the finite wavelength is felt through the second and third terms on the right at and beyond the order $\nu k_i^2 \overline{\zeta_0^2} y$ and $\nu k_r^2 \overline{\zeta_0^2} y$ respectively. The other source of $\overline{\zeta^2}$, the average rate of transfer from the mean vorticity $-U'$, constitutes the first term on the right. Since the lowest term in v is 90° out of phase with ζ_0, $\overline{v\zeta}$ starts with $y^3\overline{\zeta_0^2}\, k/6S$ and since $U'' \approx -y^2$ in Blasius layers, this transfer rate is actually negative near the wall and of order $k\overline{\zeta_0^2} y^6/S$. (For fully developed TS waves, unpublished numerical solutions of F. R. Hama and H. Fasel indicate that $\overline{v\zeta}U''$ opposes growth of $\overline{\zeta^2}$ up to the critical layer where ζ changes phase by π across the locally dominant viscous layer of Tollmien.) When this field source of $\overline{\zeta_{TS}^2}$ contributes to the receptivity, its effects should be traceable in the developing response field at heights y not yet influenced by the diffusive contribution from the wall sources. Early growth of ζ_{TS} beyond the critical layer was in fact observed in unpublished numerical experiments by H. Fasel.

2.3. *Constituents of forced solutions in unstable flows*

The behaviour of $\overline{\zeta^2}$ near a flat wall, sketched in the preceding paragraph, rests only on the basic vorticity equation (2.4) and the periodicity of the solution. Whether a solution is forced or represents a homogeneous response, it will have the limiting Stokes vorticity distribution (2.3) for small y-values. At this stage it is desirable to define what is meant by forced solutions and homogeneous (or free) response of our linear system. The terminology of forced solutions in the presence of unstable eigensolutions has not been settled. In the one *explicitly* solved, highly idealized case of an inviscid, very localized acoustic receptivity at low speeds, Bechert (1982) finds his spatially growing solution in each region composed of an 'inhomogeneous part', plus a decaying and a growing eigenfunction. We expect a superposition of more complex counterparts of the three types of solutions of Bechert: (*a*) the inhomogeneous (or particular, or forcing) solution (or field), u_f, v_f, ζ_f, p_f, imposed externally by non-homogeneous boundary conditions on our domain; (*b*) a collection of growing TS solutions, u_{TS}, v_{TS}, ζ_{TS}, p_{TS}, at the forcing frequency, which may not be in phase as they spread out from different regions along the wall; (*c*) the damped part of the homogeneous solution u_d, v_d, ζ_d, p_d (also at the driving frequency), which in principle should be constructable from the contributions of the higher damped TS modes and of the continuous spectrum as discussed by Salwen & Grosch (1981). We prefer the description 'response' to 'forced' for the additive solutions (*b*) and (*c*) of the homogeneous system. Amplified homogeneous response or free response seem both a descriptive and unambiguous characterization of the pure TS eigenfunctions measured by Schubauer & Skramstad sufficiently far downstream from their forcing vibrating ribbon.

For specific flow conditions – a given driving frequency f and a local displacement thickness δ^* – the eigenfunctions in (*b*) and (*c*) should be fixed by the dimensionless frequency $F = 2\pi f\nu/U^2$ and the Reynolds number $U\delta^*/\nu$. In principle then, for a

given F and Re_{δ^*} only the amplitudes and phases of these homogeneous solutions are unknown *a priori*. These should be determinable from the requirement that the total solution satisfies all the appropriate boundary conditions. Since an unsteady pressure gradient is a key feature of the forcing field and an unsteady vorticity the essential ingredient of the expected TS response, one would look to the no-slip wall constraint between these two fields, (2.1), to provide the link that should determine the amplitudes and phases of the eigenfunctions in (*b*) and (*c*), i.e. the complete receptivity characteristics. We believe that receptivity is most efficient when the amplitude $A(x)$ of the forcing pressure gradient has lengthscales on the order of λ_{TS}, a belief shared by Ch. K. W. Tam in his unpublished (1979) critique of the problem of receptivity to sound, and others.

2.4. *Evidence for positive receptivity*

A general proof of the preceding conjectures is likely to remain unavailable for some time. Here we shall attempt to make the conjecture plausible (*a*) by examining for constant δ the general average inputs at the wall, $(2/\rho)\overline{(\partial p/\partial x)\zeta}$, and in the field, $\overline{v\zeta}U''$, in equation (2.6) and (*b*) by invoking the results of an unpublished, specially designed numerical experiment by Hermann F. Fasel. Most importantly, the results of previous reliable experiments, as well as our own, should be consistent with the conjectures, including the $A(x)$ scaling requirement. Thus, in our experiments, even though the forcing pressure field is three-dimensional, the measured profiles $u'(y)\exp i\phi(y)$ should be expected to be Stokes-like far upstream, corresponding to u_{f}. The $u'(y)$ profiles should acquire an increasing $u'_{\max}$ at higher y-locations as substantial u_{TS} contributions appear when Re_{δ^*} exceeds the critical value for the given F. In experiments at substantially subcritical conditions, the full signal should consist of u_{f} and u_{d}, and depart little from the Stokes behaviour to be consistent with the preceding conjectures. Finally, whenever the TS contribution grows enough to become dominant near the wall, the phase velocity $\partial\phi/\partial x$ of the total signal at its maximum near the wall should approach the TS phase speed for the given F and Re_{δ^*}; for small variation of the slope about k_{TSr}, see (3.1*b*) and the discussion in §4.3. Unfortunately, none of the earlier experiments, including those of Aizin & Polyakov (1979), documented the crucial development of the $u'(y)$ and $\phi(y)$ profiles. The best results, such as those in figure 1, give only the x-variation at an unspecified height (possibly that for $u'_{\max}$). These results are consistent with the superposition of fields (*a*), (*b*) and (*c*); furthermore, x-scales on the order of TS scales are provided by the leading and trailing edges of the protruding Mylar tape.

Each of the sets of fields, such as ζ_{TS}, v_{TS}, etc., satisfies separately the basic vorticity equation (2.4). Equation (2.4) being linear and homogeneous, can also be written for the sum of the f- and TS-fields. Multiply this equation by ζ_{TS}, average over one period and consider the region above the Stokes layer where ζ_{f} vanishes: the result is an expression for the local growth of $\overline{\zeta_{\mathrm{TS}}^2}$ which contains a *non-homogeneous* term $\overline{v_{\mathrm{f}}\zeta_{\mathrm{TS}}}\,U''$ besides all the terms pertaining to the TS field alone. While the differential equation is not very useful by itself, it shows that physically there should be a direct non-homogeneous, non-diffusive input from the forcing field to the TS vorticity field throughout the boundary layer. (The coupling in the linear homogeneous equations (2.4) takes place through the boundary conditions alone; coupling in the nonlinear averaged total enstrophy equation (2.6) occurs throughout the region, clarifying the physical mechanisms at work.) If the average in x of $\overline{v_{\mathrm{f}}\zeta_{\mathrm{TS}}}\,U''$ does not vanish, the direct forced conversion of mean vorticity to unsteady vorticity $v_{\mathrm{f}}\,U''$ in conjunction with even weaker pre-existent TS vorticity, ζ_{TS}, does generate an

increment $\Delta\zeta_{TS}$ beyond the self-induced growth rate $-k_{TSi}$. Similarly the average cross-product $\overline{\zeta_{TS}(\partial p/\partial x)_f}$ at the wall could, under certain conditions, contribute to local $\Delta\zeta_{TS}$ above the self-exciting TS growth.

Let us first consider the conditions that would allow the wall input to contribute non-vanishing forced increments to the growth of $\overline{\zeta_{TS}^2}$. For a flat plate and the long-wave limit of the problem, the outer forcing field of Goldstein (1983) and Murdock (1980) is $(1/\rho)\partial p/\partial x = -\partial u/\partial t = (A/\rho)\exp(-i\omega t)$. The wall input rate in (2.6) then becomes

$$(2A/\rho)\overline{|\zeta_{TS}(0)|\exp i\{\phi_{TS}(0)\}\exp i(k_{TS}x-\omega t)\exp(-i\omega t)}$$
$$= (2A/\rho)|\zeta_{TS}(0)|\exp(-k_{TSi}x)\cos\{k_{TSr}x+\phi_{TS}(0)\}. \quad (2.7)$$

For neutral conditions the wall input (2.7) is purely oscillatory and averages out to zero over a TS wavelength. Otherwise this local average is oscillatory and of first order in the small ratio $r = k_{TSi}/k_{TSr}$, namely

$$2|\zeta_{TS}(0)||1/\rho\,\partial p/\partial x|_0\exp(-k_{TSi}x)\sin\{k_{TSr}x+\phi_{TS}(0)\}r+O(r^2).$$

A shift of the origin of x to the nearest point where the net argument of $\zeta_{TS}(0)$ vanishes, $\phi_{TS}(0)+k_{TSr}\Delta x = 0$, renders the average of second order in r and still oscillatory. Thus this rate is negligible compared to the TS self-exciting feedback rate at the wall:

$$(1/\lambda)\int_{x-\frac{1}{2}\lambda}^{x+\frac{1}{2}\lambda}(2/\rho)\overline{(\zeta\,\partial p/\partial x)_0}\,dx$$
$$= |\zeta(0)||(1/\rho)\,\partial p/\partial x|_0\cos\{\phi_\zeta(0)-\phi_{px}(0)\}\exp(-2k_{TSi}x). \quad (2.8)$$

Consider now a forcing pressure gradient with an amplitude $A(x)$ varying along the flat wall, the case corresponding more closely to our local sound source located above the boundary layer. Let the Fourier transform of $A(x)$ be $A_F(k)$, so that $(2\pi)^{\frac{1}{2}}A_F(k) = \int_{-\infty}^{+\infty}A(x)\exp(ikx)\,dx$. The averaging is now modified; if $A(x)$ makes a non-zero contribution $\Delta A_F(k_{TS})$ at the TS wavenumber between $x-\frac{1}{2}\lambda$ and $x+\frac{1}{2}\lambda$, there arises a net local input rate from the forcing field to the TS $\overline{\zeta^2}$ field per cycle, per unit area, of magnitude

$$\frac{1}{\lambda}\int_{x-\frac{1}{2}\lambda}^{x+\frac{1}{2}\lambda}\frac{2}{\rho}\overline{\zeta_{TS}(0)\left(\frac{\partial p}{\partial x}\right)_f}\,dx = \frac{|\zeta_{TS}(0)|}{\rho}\frac{k_{TSr}}{(2\pi)^{\frac{1}{2}}}\mathrm{Re}\{\Delta A_F(k_{TS})\}. \quad (2.9)$$

The increment $\Delta A_F(k_{TS})$ in effect reflects the commensurability of λ_{TS} and the local characteristic length introduced by the amplitude variation $A(x)$ of the forcing unsteady pressure gradient. Using properties of Fourier transform, $\Delta A_F(k_{TS})$ can be expressed as $\exp(-k_{TSi}x)A_F(k_{TSr})\Delta k/k_{TSr}$, where Δk represents a generalized bandwidth. In either case, evaluations of (2.9) in specific cases have to be numerical.

The contribution of $\overline{v_f\zeta_{TS}}\,U''$ to the $\overline{\zeta_{TS}^2}$ growth rate is similarly non-zero when the harmonic pressure gradient varies as $A(x)$. First, and most importantly, the $A(x)$-dependence builds up the v_f motion very rapidly in proportion to and on the scales of $A'(x)$. As a consequence of the continuity equation the amplitude of v_f is proportional to $A'(x)+ik_fA(x)$ – say $V_f(y)\{A'(x)+ik_fA(x)\}$. Because the $A'(x)$-term is in phase with ζ_0, the $\int_0^y\overline{v\zeta}U''\,dy$ contribution in (2.6) now commences with the fifth power of y at the wall. For the long-wavelength limit, only the $A'(x)$-term is present and upon integration over λ_{TS} yields proportionality to $-ik_{TS}\Delta A_F(k_{TS})$ in the form:

$$\frac{1}{\lambda}\int_0^y\int_{x-\frac{1}{2}\lambda}^{x+\frac{1}{2}\lambda}\overline{v_f\zeta_{TS}}\,U''\,dx\,dy = \frac{k_{TSr}}{2(2\pi)^{\frac{1}{2}}}\int_0^y\mathrm{Im}\{k_{TS}\Delta A_F(k_{TS})\zeta_{TS}(y)\,V_f^*(y)\}\,U''(y)\,dy. \quad (2.10)$$

The alternative expression for (2.10) is obtained by replacing $\Delta A_F(k_{TS})$ inside the Im operator by $\exp(-k_{TSi}x)\,A_F(k_{TSr})\,\Delta k/k_{TS}$. Other comments on (2.9) remain valid here. Conditions (2.9) and (2.10) refer to local conditions within $\frac{1}{2}\lambda_{TS}$ from x. At more distant x-locations new contributions may not be in phase with the initial ones and partial cancellations of response may take place. Such negative contributions will be evident in our experimental cases S, U and N, but not in case U_w.

The preceding arguments can be generalized to forcing excitations by pressure fields moving at 'convective' speeds below or at the free-stream speed, such as those due to unstable wake streets indicated schematically in figure 3. Let the wake frequency be ω, the wavenumber k_w and the amplitude $A_w(x)$. When A is constant, $\cos\{k_{TSr}x+\phi_{TS}(0)\}$ in (2.7) is replaced by $\cos\{(k_{TSr}-k_w)x+\phi_{TS}(0)\}$. All the comments following (2.7) can be paraphrased with λ_{TS} replaced by $\lambda_{TSw}=2\pi/(k_{TSr}-k_{wr})$. Similarly in the case of variable amplitude $A_w(x)$, the expression $(k_{TSr}-k_{wr})\,\Delta A_{wF}(k_{TS}-k_w)$ takes the place of $k_{TSr}\,\Delta A_F(k_{TS})$ in (2.9) for the local contribution to the spatial growth of $\overline{\zeta_{TS}^2}$ by the forcing effect of the propagating pressure field of the unstable wake.

Evidently the difference in propagation speeds does not matter, as long as the variable amplitude can supply characteristic wavenumbers commensurate with the difference in wavenumbers $k_{TSr}-k_{wr}$. This should not be surprising since in the long-wavelength limit $k_f\to 0$ of the fixed exciting source there was also a mismatch in propagation speeds. Our fourth experimental unstable case U_w, described in §3, deals with a combination of the fixed source and moving-wake sources, where these concepts are applicable.

Besides the experimental results of §4, the most direct evidence for the mechanisms discussed in §2 is found in the unpublished numerical experiment of Hermann Fasel. Space does not permit detailed description nor inclusion of figures of the evolving total fields u, v, and ζ obtained by Fasel's (1976) techniques. Suffice it to say that the ability to start and stop the forcing field instantly brought out clearly (i) early TS vorticity growth diffusing from the wall sources, and (ii) early growth of ζ_{TS} at heights y which could not have been due to diffusion from the wall. The features of effect (ii) are completely consistent with the input $\overline{v_f\zeta_{TS}}\,U''$ described in §2.2.

3. Experimental considerations

We decided to maximize the localization of the pressure field by bringing the successful movable, Pitot-like three-dimensional sources of Morkovin & Paranjape (1971) into the free stream close to the boundary layer formed on the back wall of the IIT Visualization Facility. Consequently, the controlled forcing fields were very low in intensity and decayed to ineffectual levels within a fraction of the acoustic wavelength λ_{ac}, within or outside of the TS-amplifying domain. As a result, the effective acoustic field of the primary source was dominated by the near field, i.e. it was given to a good first approximation by a fixed incompressible harmonic source in a fluid moving with U_e and its reflection from the tunnel walls. The low intensity of the field avoided completely pitfall (iv) described in §1; all the experiments were run below any onset of nonlinearity in the overall forcing and response system. *The linearity of the response was checked repeatedly.* The pressure field was so low that we could only tell whether the source was on or off by monitoring the excitation and response voltages. In other tests of receptivity, the experimenters had to contend with fatigue caused by the exposure to high-level sound.

The rapidly decaying forcing field also precluded build-up of acoustical and mechanical resonances. A subsequent experiment by Bar Sever (1984) in which the

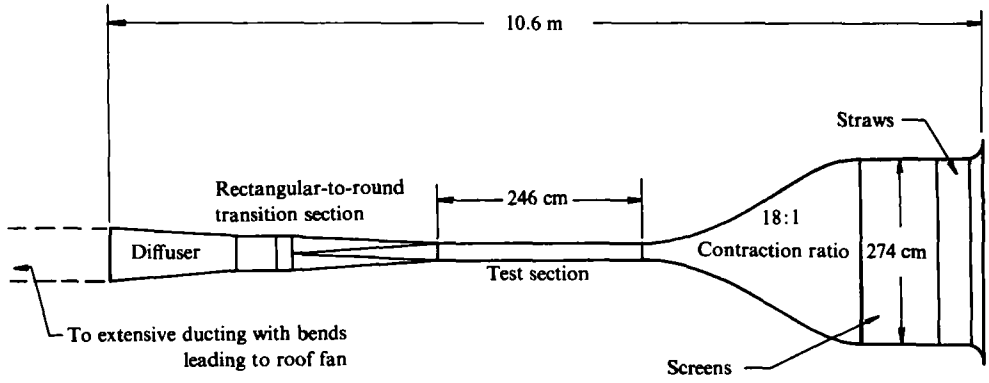

FIGURE 2. Schematic top view of IIT open-throat Visualization Facility with two-dimensional 18:1 contraction. The basement facility was exhausted to the atmosphere through a 1.83 m fan on the second-floor roof, about 25 m distant from the end of the diffuser.

pressure field was imposed directly by a loudspeaker mounted at the upstream end of the front wall of the same test section demonstrated *a posteriori* the advantage of the adopted local sources. Bar Sever's limited objective of stimulated growth of TS waves was achieved, but detail quantitative interpretation was marred by non-monotonicity of the response with respect to the excitation frequency. Complex discrete resonances of the acoustic and overall mechanical system (including probe support) were superposed upon the desired direct TS-wave response to the speaker source field. A similar non-monotonic peaky TS response in the receptivity experiments of Spangler & Wells (1968) was criticized in the aforementioned Soviet surveys by Ginevskii *et al.* (1978) and Kachanov *et al.* (1982).

The test boundary layer was formed on the back wall of the IIT open-throat Visualization Facility, figure 2, downstream of a two-dimensional 18:1 contraction from a 73.7 cm × 274 cm rectangular settling chamber. This configuration avoided therefore pitfall (iii) of §1 – the singular fields associated with the vibrations of the leading edge and with the sharp local diffraction fields around the edge due to imperfect alignment of exciting sound fields. The measured boundary-layer profiles corresponded very nearly to flat-plate Blasius solutions with displacement thicknesses from 2 to 2.5 mm and with effective leading-edge locations in the contraction of the tunnel. Since the relevant Tollmien critical heights ranged from 1.3 to 1.6 mm, hot-wire traverses from about 0.3 mm outward provided the required type of local information on $u'(y)$ and $\phi(y)$ mentioned under (ii) in §1. The crucial vorticity information, however, was unobtainable and can only be inferred indirectly in special regions. Neither could hot-wire anemometry at the low excitations in our relatively thin layers supply sufficiently accurate information on the v-fluctuation component which plays the important role outlined in §2.4.

The mean and fluctuation velocities were measured by standard linearized hot-wire anemometry. The probe, made of tungsten wire, was 4.5 μm in diameter and 1.5 mm in sensitive length. The r.m.s. level of the u-fluctuation, u', in the test section did not exceed 0.1 % of free-stream velocity U_e, with about 90 % of the signal registered below 25 Hz. Thus the relative spectral disturbance level was small, below 0.003 %, in the 30–80 Hz range of interest. Spectral measurements of fluctuating static pressure were nearly proportional to hot-wire sensed u' according to the linearized Bernoulli equation; this indicates that the bulk of the disturbances consisted of

large-scale, low-frequency (near-field) pressure fluctuations, rather than of finer-scale convected turbulent vortical fluctuations. Dominance of u'/U_e by low-frequency pressure fluctuations seems to be common in open-throat wind tunnels with quiet driving fans. The free-stream spectra decreased steadily from the lowest registered frequency but did have small relative maxima near 11 Hz and 22 Hz, corresponding to the lengthwise and crosswise acoustic resonances of the laboratory room. In the forcing experiments, the u-fluctuation at the excited frequencies was always band-pass filtered from the total to obtain good accuracy in the measurement. The y-distributions of the mean velocity $U(y)$, the r.m.s. u-fluctuation $u'(y)$ and the phase $\phi(y)$ were all recorded on an $X-Y$ recorder simultaneously during each traverse. The phase was measured by a phase meter. The full and filtered signals were monitored on an oscilloscope at the beginning and end of a traverse or more often.

As mentioned in the Introduction, the scheme of localizing the oscillating pressure field through a movable local source introduced one serious complication into the experimental set-up. The piping that carried the fluctuations from the speaker diaphragm to the Pitot-static opening in the free stream generated wakes in the test section. These wakes also responded to the excitation field and in turn produced secondary unsteady travelling pressure sources at the excitation frequency. (In the Morkovin–Paranjape 1971 jet experiments the local forcing source was located outside the flow region and therefore caused no wakes and associated complications.) Starting with the 1971 Pitot-like source configuration, long months of experimentation with different support systems and with different partial shielding plates led us to the configuration sketched to scale in figure 3. Each of the tested configurations made us more appreciative of the complexities of acoustic forcing of wakes and their pressure interactions.

The sound was ducted from a woofer-type loudspeaker (of about 30 cm in diameter) through a multiply bent pipe with outer diameter of 0.6 cm to a Pitot-static-like elliptic head, with its tip positioned at station $x = 0$. Two holes of diameter of 0.2 cm, with centres lined up parallel to the wall, constituted the actual source geometry. They were located 28 mm downstream from the elliptic tip and 76 mm upstream of the 10° bend of the ducting, which commenced at station 104 mm. The 1 mm thick wake-shielding plate with rounded edges was positioned 10 mm (toward the wall) from the centres of the sound holes, with its leading edge 2.5 mm downstream of the centres. The spanwise width of the plate was of 37 mm between $x = 30.5$ and 94.5 and of 109 mm between $x = 94.5$ and 131.5. This was the standard configuration which decreased substantially the influence of the wakes and of the convected disturbed fluid ejected out of the holes over half of each period. For the most disturbed condition in figure 6 the shielding plate was absent; for the condition in figure 10 the plate was made to shield the direct source by moving its leading edge to $x = -53$ and extending its length to $x = 48$.

Comparison between responses at a fixed velocity U_e and frequency f in shielded and unshielded configurations provided an appreciation of the unwanted wake effects. Contrasts between responses for identical source-and-shielding geometry at different speeds U_e and frequencies f, i.e. for different conditions of TS growth, yield insight into the basic characteristics of boundary-layer receptivity in §4. Three conditions were chosen for the source tests with the 180° phase change under the source: the very stable case S, with forcing at 50 Hz at $U_e = 3.3$ m/s; the 'just stable' case N, with forcing at 30 Hz at the same speed of 3.3 m/s; and the unstable case U at $U_e = 7.3$ m/s with forcing at the same frequency of 30 Hz. The three cases S, N and U test the relative development, or lack of it, of the three constituent fields

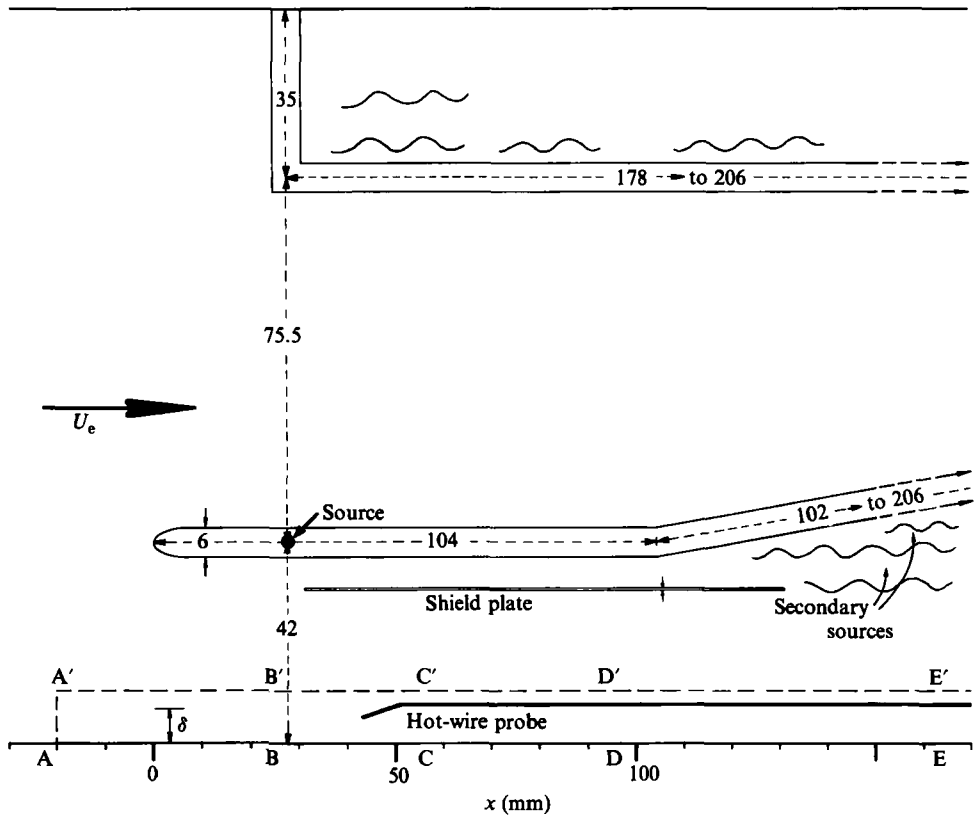

FIGURE 3. Primary configuration (to scale) of acoustic Pitot-static source and the shield plate in the excitation of the sidewall boundary layer. Dimensions in mm.

$( )_f$, $( )_d$, and $( )_{TS}$ discussed in §2.3. A fourth case U_w, for the unstable 7.3 m/s condition, with the shield plate moved 83.5 mm upstream to block the forcing excitation upstream of the source, was chosen to document TS-wave growth without the 180° phase change in u_f under the source. Except for the presence of moving secondary sources in the wake, this case corresponds to the more commonly occurring acoustic receptivity configurations, such as that of Kegelman (1982).

The forcing field for the cases S, N, and U is defined by measurements of $u'(x, y)$ and $\phi(x, y)$ along the contour AA′B′C′D′D and for case U_w along CC′D′E′E in figure 3. At the front boundaries AA′ and CC′ the input profiles are found to be essentially Stokes-like, as (2.2*b*) suggests for the upstream end of the interaction region. At the downstream boundaries, the profiles generally include u'_d and especially u'_{TS} components; however, an appropriate u'_f Stokes profile can be constructed approximately from $u'_f(D')$, as the stable case S confirms. If the fields were two-dimensional, the above specifications would be sufficient in principle to determine the inviscid forcing field and its viscous sublayers at A and D. The three-dimensionality of our primary forcing source helped to reduce considerably the size of the region of significant receptivity, but it did complicate the empirical definition of the forcing field. Since the main conceptual issue here is the effect on receptivity of the x-variation in the amplitude $A(x)$ of the unsteady pressure gradient, none of our probing in the z-direction is reported. The $A(x)$ variation is provided adequately by traverses along A′B′C′D′E′.

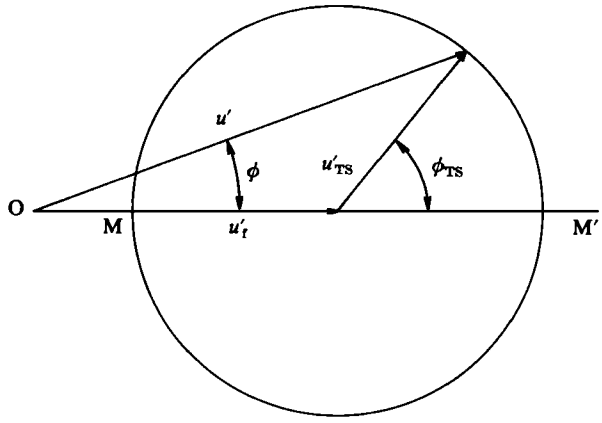

FIGURE 4. Vectorial representation (3.1) of total measured signal u' composed of a stationary forcing field $u'(x,y,t) = u'_{\rm f}\exp(-{\rm i}\omega t)$ and a pure TS response $u_{\rm TS}(x,y,t) = u'_{\rm TS}\exp{\rm i}(k_{\rm TS}x-\phi_{\rm TS0})\times\exp({\rm i}\omega t)$, where $u'_{\rm f}$, $u'_{\rm TS}$ and $\phi_{\rm TS} = k_{\rm TS}x-\phi_{\rm TS0}$ are functions of x and y.

The interpretation of the empirical amplitude development $u'(x,y)$ and phase variations $\phi(x,y)$ of the total signal must rest on the conceptual model of its components, say that described in §2.3. The approach can be illustrated for the simpler case of local dominance by a stationary forcing field $u_{\rm f} = u'_{\rm f}\exp(-{\rm i}\omega t)$ and by a TS response field $u'_{\rm TS}\exp({\rm i}\phi_{\rm TS})\exp(-{\rm i}\omega t)$. Here $\phi_{\rm TS}(x,y)$ is the relative phase of the evolving TS response with respect to the phase of $u_{\rm f}$ as depicted in the complex plane of figure 4. Only beyond the region of genesis of the TS response can the phase $\phi_{\rm TS}$ be related to the phase development of the fundamental normal mode: $\phi_{\rm TS}(x,y) = k_{\rm TSr}x+\phi_{\rm TS0}$. Hot-wire and phase-meter measurements provide $u'(x,y)$ and $\phi(x,y)$ of the total field, which in accordance with figure 4, is expressible as

$$u'\exp({\rm i}\phi) = u'_{\rm f}(x,y)+u'_{\rm TS}(x,y)\exp({\rm i}\phi_{\rm TS}), \tag{3.1a}$$

$$\tan\phi = \frac{\sin\phi_{\rm TS}}{p+\cos\phi_{\rm TS}}, \tag{3.1b}$$

$$\left(\frac{u'}{u'_{\rm TS}}\right)^2 = p^2+1+2p\cos\phi_{\rm TS}. \tag{3.1c}$$

Here $p(x,y)$ is the generally variable relative strength of the forcing amplitude $u'_{\rm f}$ to the local response amplitude $u'_{\rm TS}$ at any point in the field. Past the region of genesis, the expression for the normal-mode amplitude: $u'_{\rm TS}(x,y) = u'_{\rm TS}(x_0,y)\times\exp\{-k_{\rm TSi}(x-x_0)\}$ should be applicable and incorporated into (3.1), in particular in the p-terms. From this expression and (3.1c), it is clear that in the region of pure self-excited growth the measured u' has a distorted undulation with a wavelength of $\lambda_{\rm TS}$ and a relative amplitude of p superposed on the normal-mode growth $\exp\{-k_{\rm TSi}(x-x_0)\}$. As p diminishes to zero, the undulation in measured u' disappears. It is possible to generalize (3.1) to the case of forcing by a non-stationary wake pressure field characterized by $u_{\rm f} = u'_{\rm w}(x,y)\exp{\rm i}\phi_{\rm w}$, where $\phi_{\rm w}$ is likely to vary as $k_{\rm wr}x-\phi_{\rm w0}$. In (3.1$b$, c) we simply replace ϕ by $\phi-\phi_{\rm w}$ and $\phi_{\rm TS}$ by $\phi_{\rm TS}-\phi_{\rm w}$. The resulting undulation in measured u' should undergo an undulation of wavelength $\lambda = 2\pi/(k_{\rm TSr}-k_{\rm wr})$ beyond the region of active local stimulation of TS waves.

The representation (3.1) provides ready interpretation of figure 1, due to Aizin & Polyakov (1979), where the TS growth is documented over many TS wavelengths

relative to a nearly constant-amplitude u_f'. The minima and maxima in figure 1 correspond to segments OM and OM′ in figure 4. In contrast to figure 1, our receptivity study (except for the smoke-wire visualization of figure 5) is concerned with the region of genesis of u_{TS}; in figure 1 such a region is upstream of $x = 0.59$, where Aizin & Polyakov give no coherent information. In this region the superposition should include the damped response u_d and the increments in the TS wave Δu_{TS} due to local strengthening through the input from the non-homogeneous solution.

4. Experimental results and discussion

4.1. *The smoke-wire evidence*

Figure 5 presents a smoke-wire visualization of the spatial growth of a three-dimensional TS-wave formation generated by our early unshielded Pitot-like source at 30 Hz located just outside of the boundary layer in a free stream with $U_e = 5.5$ m/s at $x = 0.2$ cm, $y = 0.8$ cm and $z = 0$. The three-dimensional excitation generates not only ζ-vorticity through oscillatory $\partial p/\partial x$ in accordance with (2.1), but also streamwise vorticity ξ through oscillatory $\partial p/\partial z$. In figure 5 the smoke accumulation in Kelvin's cat's eyes is observed over about one-third of the TS wavelength of approximately 7.5 cm. The propagation speed λf at 30 Hz is approximately $0.075\ \text{m} \times 30(\text{s})^{-1} = 2.25\ \text{m/s} = 0.41 U_e$. The spurious incremental effect of the smoke-wire wake described by Thomas (1984) is completed upstream of the source so that the growth in intensity and spanwise extent of the wave packet seen in figure 5 should represent the true TS response to the forcing fields. Here these fields include unknown secondary pressure sources from the stimulated modulated wakes that were generated by cylindrical piping centred on $x = 0.2$ cm (diameter of 6.35 mm for $8.9 < y < 15.2$ cm pared to a diameter of 1.59 mm for $0.8 < y < 7.6$ cm. The forcing fields and the decaying part of the homogeneous response, of course, do not contribute directly to the discernible accumulation of the smoke in figure 5.

From hot-wire measurements of the boundary-layer profiles for $20 \leqslant x \leqslant 40$ cm at $U_e = 7.3$ m/s, a displacement thickness δ^* of approximately 2.64 mm was inferred for the conditions in mid-figure 5. The Reynolds number based on this displacement thickness is 970. At this Reynolds number a two-dimensional TS wave at the given dimensionless frequency $\omega\delta^*/U_e = 0.091$ travels at $0.352 U_e$ and has a wavelength of 64 mm according to charts of Wazzan, Okamura & Smith (1969). The propagation speed and wavelength of the wave in figure 5 are therefore approximately 16% and 17% larger than the two-dimensional TS wave at the driving frequency. Clearly, TS waves of different obliquities, corresponding to the same fixed frequency of 30 Hz, are superposed on the two-dimensional free response. According to charts for oblique waves of Gaster (1977), obliquity increases streamwise propagation speed and wavelength, in agreement with the results of figure 5.

4.2. *The forcing fields and the stable case S*

The forcing non-homogeneity, i.e. experimental variations $u_f'(x, 11\ \text{mm})$ and $\phi_f(x, 11\ \text{mm})$ beyond the boundary layer δ of approximately 7 mm for the stable and unstable cases S and U, are presented in figure 6 for the interaction region associated primarily with the source forcing and the shield geometry of figure 3. Measured representative $u'(y)$ and $\phi(y)$ profiles, which combine the forcing and response fields, are shown in figure 7 for case S. Comparable profiles for case U are displayed in figures 8(*a–d*). Stokes-like initial profiles at $x = -10$ in figures 7(*a*)(i), (*b*)(i) for case S, and at $x = -30$ in figures 8(*a*, *d*) for case U complete the definition of the forcing

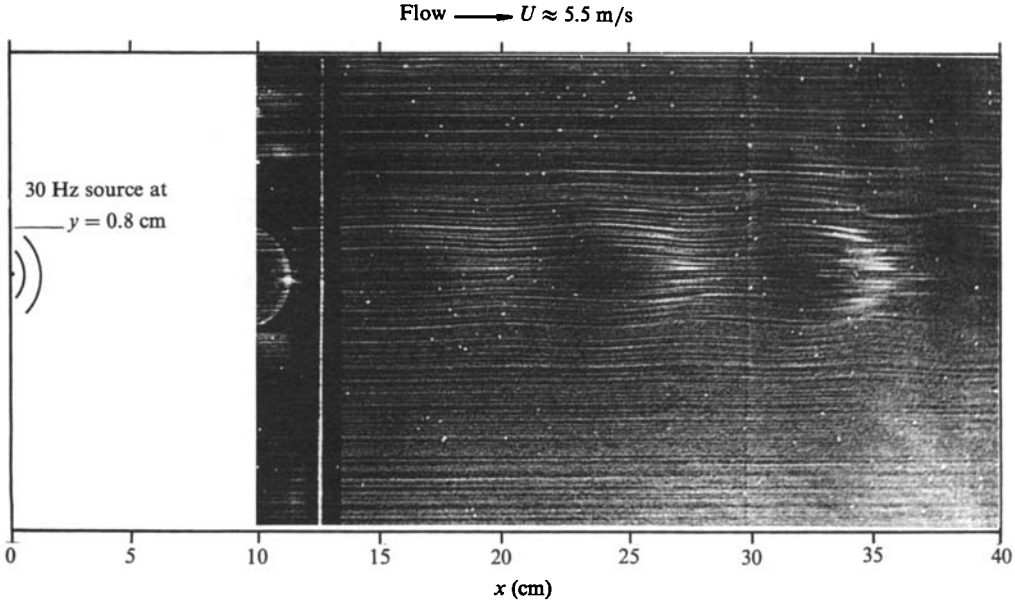

FIGURE 5. Smoke-wire visualization of the TS formation and growth excited by a shieldless Pitot-like source at 30 Hz located at $x = 0.2$ cm, $y = 0.8$ cm, $z = 0$ in a 5.5 m/s stream.

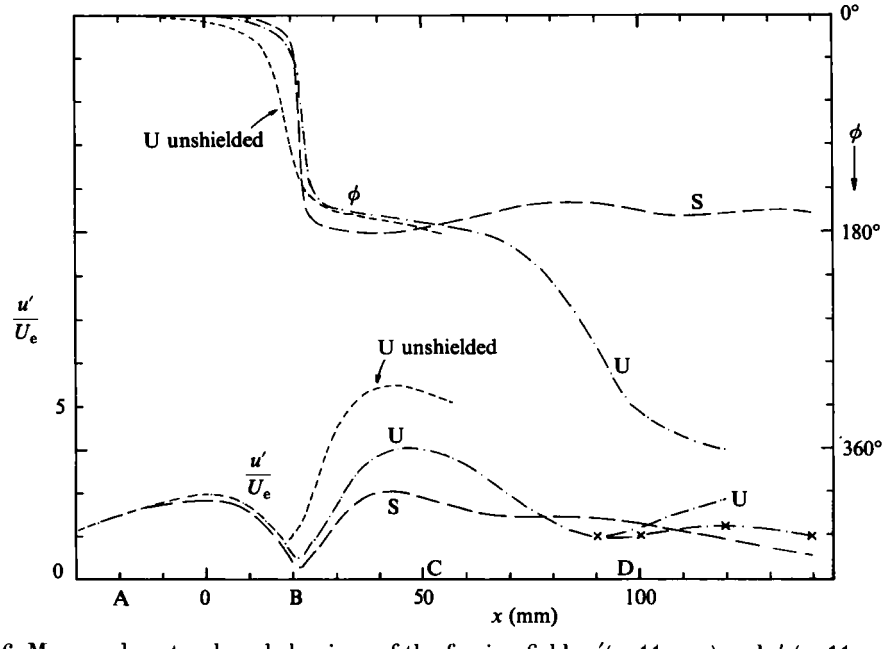

FIGURE 6. Measured centreplane behaviour of the forcing field, $u'_f(x, 11\text{ mm})$ and $\phi_f(x, 11\text{ mm})$ for the stable case S: 50 Hz, 3.3 m/s; and the unstable case U: 30 Hz, 7.3 m/s, for source position $x = 28$ mm, $y = 42$ mm $= 6\delta$ and shield configuration of figure 3; also for unstable case with shield plate removed. The u'/U_e scales in figures 6–10 are arbitrary; linearity was verified for each experiment.

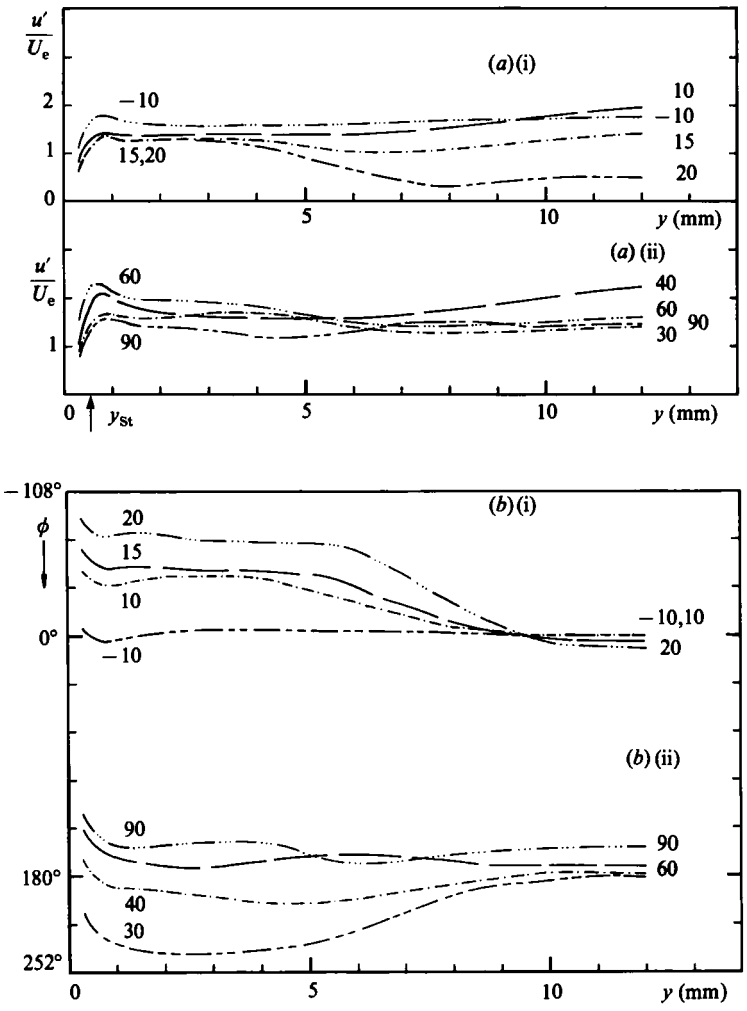

FIGURE 7. Development in x (in mm) of y-profiles of (a) total signals u' and (b) ϕ for the stable case S: $F = 4.2 \times 10^{-6}$, $\delta^* = 2.5$ mm, $Re_{\delta^*} = 550$, theoretical Stokes overshoot $y_{St} = 0.74$ mm.

functions on segments AA′ of figure 3, as discussed at the end of §3. Figures 6 and 7 of Loehrke *et al.* (1975) give y_{St}, the y-position of the maximum in the Stokes layer superposed on a Blasius layer, approximately at $2.4S$ at a lag of approximately 50° from the wall limit, i.e. 5° from u_f at $6S$; for cases S and U the expected locations of the overshoot are therefore 0.74 mm and 0.96 mm respectively. Note the differences in the range of the smoke-wire figure 5, measured in cm, and the range in figures 6 and 3, measured in mm. In contrast to figure 5, we are now focusing on the early and main region of the forcing, not previously reported in research literature.

The forcing field $u'_{fS}(x)$ in the stable case in figure 6 exhibits near symmetry with respect to $x = 22$ rather than $x = 28$, the abscissa of the source at height $y = 42$ mm. The 180° phase change at $y = 11$ takes place between stations 6 and 40, primarily near 22. (Strictly speaking, symmetry in u' and a π change in ϕ would make the forcing field antisymmetric.) Since u'_{fS} continued to decrease to $x = 155$ at essentially constant $\phi_f(x)$, pressure radiation from the unstable wakes was effectively postponed beyond the x-range of our study at this low velocity of 3.3 m/s. The slight asymmetry

in $u'_{fS}(x)$ therefore must stem from some combination of (*a*) asymmetry due to the shielding plate, (*b*) differences between the probably symmetric suction stage and the asymmetric ejection stage of the pumping cycle at the two orifices constituting the physical pressure source, and (*c*) the inherent field asymmetry of a fixed ideal source in a moving fluid. The slightly decreased phase lag ϕ_{fS} for $x > 40$ points to the distorted fields around the shielding plate as the major contributor to the asymmetry in the case S.

In the unstable case U at 7.3 m/s the additional contribution due to the pressure fields from the excited wakes influences the forcing field at $y = 11$ mm. This is indicated by the changes in the slope of $\phi_{fU}(x)$ for $x > 30$ and especially for $x > 70$; here, outside the boundary layer, (3.1*b*) is applicable with the subscript w for wake substituted for the subscript TS. With the shield removed, the wake contribution evidently grows further as can be judged from the third set of curves in figure 6. It is especially significant that the two $u'_{fU}(x)$ variations coincide, within experimental error, upstream of $x = 12$. Clearly the wake and shield effects do not reach there, and the early variation well past the first maximum near $x = 2$ mm must characterize the fixed primary-excitation source alone. As the additional wake sources are superposed the asymmetry of $u'_{fU}(x)$ with respect to the minimum increases and with it the value of u'_{min} itself.

We note that the linearity of the responses allows us to change the ordinate of any u' variation in x or y by a constant factor for the purposes of comparison, say in figure 6. Thus the forcing variations $A(x)$ in the shielded S and U cases upstream of $x = 20$ are seen to be little affected by the changes in frequency from 50 to 30 Hz and in U_e from 3.3 to 7.3 m/s. In this region, then, we can expect the receptivity developments due to the forcing-amplitude variations $A(x)$ associated with a three-dimensional fixed source to be rather general. In the following region BB′C′C of figure 3, we can look for the major effects on u_U of the early antisymmetric part of $A(x)$, i.e. the negative interference effect according to (2.9).

The causes of the $u'_{fU}(x, 11\text{ mm})$ variations past DD′ are unclear but most likely correspond to secondary forcing sources in the wakes which are difficult to reproduce. Thus $u'_{fU}(x, 11\text{ mm})$ at $x = 90$, 100, 120 and 140 in figure 6 marked by × symbols were measured for the nominally identical conditions in an experiment four months before the more detailed U-case results of figure 8. Analysis of profiles for $x > 90$ points to non-reproducibility of the wake-induced pressures as the cause. Had we not monitored the forcing function $u'_f(x, 11\text{ mm})$, the effect would have remained mysterious, as do many phenomena reported in the literature on acoustic receptivity. A detailed discussion of the behaviour of the fields past $x > 90$ in terms of (3.1) is available from the second author.

Theoretically, a two-dimensional TS wave at $Re_{U\delta^*}$ of 1120 corresponding to $f = 30$ Hz and $\delta^*_U = 2.3$ mm near the source, would have a TS wavelength λ_{TSU} of about 78 mm and a propagation speed c_{rU} of $0.32U_e$. Our documented region therefore covers about 1.5 TS wavelengths in the unstable configuration U, stopping just short of where figure 5 takes up with visual evidence. Extrapolation of charts for the stable case S with $\delta^*_S = 2.5$ mm near the source at 50 Hz and U_e of 3.3 m/s, yields a two-dimensional wavelength λ_{TSS} of 30 mm and propagation speed of c_{rS} of $0.45U_e$ at $Re_{S\delta^*}$ of 550. The just-stable case N differs from case S only in the forcing frequency $f = 30$ Hz, which lengthens the theoretical two-dimensional response wavelength to 46 mm and slows down the propagation speed to $0.40U_e$.

The striking common feature of the u'_S profiles in figures 7(*a*)(i) and (ii) is the overshoot at y near 0.7–0.8 mm followed by a fairly constant u'_S value up to 3–4 mm.

As already noted in connection with the initial profile at $x = -10$, y_{St} of the overshoot at 50 Hz should occur near 2.4S, i.e. near 0.74 mm; the asymptotic value is usually reached beyond 6S, i.e. past 1.9 mm. The phase advance from y_{St} toward the wall is also evident, but more difficult to compare with the expected 50° value because of uncertainties in extrapolation and in smoothing of increased jitter near the wall. Thus, for thc stable case, not only is the upstream inner profile Stokes-like, but so are the subsequent inner profiles responding to the changes in the driving amplitude and phase at $y = 11$ mm shown in figure 6. (In seeking the link between the outer and inner profiles we should keep in mind that the hot-wire traverses describe fixed-x characteristics; on physical grounds the usage of bipolar coordinates centred on the effective source and its reflection in $y = 0$ would be more appropriate.) For the fixed-x traverses in figures 7(*b*)(i) and (ii) the inner $\phi_S(y)$ profiles advanced in an orderly fashion as x increased: the apparent jump between $x = 20$ and 30 really corresponds to a smooth, continuous in-phase shift from 0 to 2π between $x = 20$ and 24. (Unfortunately the $\phi_S(y)$ profile at $x = 24$ is missing, but the feature under discussion is well reproduced by $\phi_U(y)$ at $x = 24$ in figure 8*d*.)

The real 180° shift, which corresponds to the change in direction of u_f near the source, takes place in a nearly discontinuous manner in the outer profiles. A cross-plot of $\phi_S(x, y)$ in figures 7(*b*)(i) and (ii) against x near the wall – say at $y = 1$ mm – gives the false appearance of a wave propagating upstream whereas we know that the dominant oscillating field is stationary. This feature reflects primarily the basic $\phi(x, y_0)$ variation of the forcing source field, with its Stokes layer, as it is accommodating to the phase change of π near the source. The exploration of the stable case S was intended to calibrate for us the essential behaviour of the dominant source component of the forcing field. In the U case we can think of the total u-field as incorporating the patterns of figure 7 as a base (augmented by the forcing wake component) on to which the continuously seeded and amplifying TS waves are grafted.

4.3. *The unstable case* U

The detail evolution of the above forcing field and the growing response is presented in figures 8(*a–d*). The inner phase profiles $\phi_U(y)$ up to $x = 30$ in the upper part of figure 8(*d*) give the impression that the initial behaviour is merely a slightly exaggerated version of the steady phase advance observed in figures 7(*b*)(i) and (ii) for case S. However, figure 8(*a*) shows that past $x = 0$ the Stokes' overshoot in the amplitude u' is overtaken by a broad and rapid u' growth in x with a maximum near y of 1.5 mm, i.e. beyond the y_{cr} location of 1.3 mm. Since this extra growth is absent in figure 7(*a*), there is little doubt that in the region AA′B′B this development must represent the non-homogeneous seeding and the free u_{TS} response to the variable forcing amplitude $A(x)$ in figure 6. According to the conceptualization described at the beginning of §1, we can expect that in principle an eigenfunction decomposition of the fluctuating field at an upstream x_0 (where the dimensionless rate $\mathrm{d} \ln A/\mathrm{d}(x/\lambda_{TS})$ becomes significant) would disclose non-vanishing strength of the fundamental mode component, $u_{TS}(x_0)$; upstream extrapolation of the $u'_f(x, 11\text{ mm})$ shapes in figure 6 suggests -80 to -120 as suitable choices for x_0. On the basis of our heuristic arguments in §2.4, local wall and mid-layer inhomogeneous inputs to the spatial growth of $\overline{\zeta_{TS}^2}$ past x_0 should take place in accordance with (2.9) and (2.10). In these equations the phase reference was normalized. When the phase reference is not adjustable at each step, the local input at x' and the resulting local increment $\Delta\zeta_{TS}(x')$ are dependent on the pre-existent local phase and are therefore complex functions of x'. A $\Delta\zeta_{TS}$ increment at any x' grows with the TS growth rate $\exp\{-k_{TSi}(x-x')\}$

past x' and the same should be true for the associated *complex* velocity-field increments Δu_{TS}. The superposition of the initial TS component growing from x_0 and the continuous forced increments with their subsequent TS growths yields

$$u_{\mathrm{TS}}(x) = u_{\mathrm{TS}}(x_0)\exp\{-k_{\mathrm{TSi}}(x-x_0)\}+\int_{x_0}^{x}\Delta u_{\mathrm{TS}}(x')\exp\{-k_{\mathrm{TSi}}(x-x')\}\,\mathrm{d}x'. \quad (4.1)$$

The u_{TS} component (4.1) ultimately becomes measurable in the presence of the stronger u_{f} field and noise. This emergence of u_{TS} from the noise evidently occurs near $x = 0$, after continuous cumulation over a distance of positive $A(x)$ and positive $A'(x)$ forcing on the order of one λ_{TSU} of 78 mm. This growth slows down beyond B where interfering inputs at the wall commence as $A(x)$ *de facto* changes sign.

In the light of the preceding interpretation of developments up to $x = 20$ in figures 8(*a*, *d*) the phase advance with x of the inner profiles for case S in figure 7(*b*)(i) (which is slower than the TS influenced advance in the upper part of figure 8*d*) may be partially related to the u_{d} and u_{TS} characteristics even though these components are damped. The non-homogeneous solution, i.e. the forcing field, even with its Stokes-like adjustment at the wall, is unlikely to satisfy all the boundary conditions by itself. But the major differences between figures 7(*a*)(i) and (*b*)(i) and figures 8(*a*, *d*) stem primarily from the change from negative to positive amplification rate, $-k_{\mathrm{TSi}}$. For negative $-k_{\mathrm{TSi}}$ the conceptual equation (4.1) indicates that the u_{TSS} component must be very small, even though it may cause part of the phase change in figures 7(*b*)(i) and (ii).

As discussed in connection with figures 7(*b*)(i) and (ii), the phase shift between stations $x = 20$ and 24 in figure 8(*d*) is really an in-phase shift, of reference, from zero to 2π, less a small continuous phase advance expected over the intervening distance of 4 mm. This phase advance in the inner layers of figure 8(*d*) continues from $x = 24$ to 30, as in figure 7(*b*)(ii) but is then overtaken by a steadily increasing lag near the wall which is essentially absent in the S case. This change of trends takes place past B, in the region of interference of new $\mathrm{d}\overline{\zeta^2}/\mathrm{d}x$ inputs with the accumulations from upstream and in the region of probable mild wake contributions to the forcing field. The relative strength of the latter is judged by the excess of the forcing function u'_{fU} over u'_{fS} along $y = 11$ mm and by the moderate slope of ϕ_{fU} in figure 6 over the segment BC. The reversal and the monotonic development of the lag $\phi_{\mathrm{U}}(y)$ from $x = 30$ to 54 in figure 8(*d*) (absent in the stable case) must be related to the activated negative inputs in this region in the presence of TS amplification. The TS phase generally lags in the downstream direction whether the amplitude is increasing or decreasing. This view is corroborated by the corresponding inner monotonic decrease in u' in figure 8(*b*) which appears to be disconnected from the forcing levels outside the boundary layer. The superposition of fields in (3.1) does not include the damped u_{d} fields; nor can the phase ϕ_{TS} in (3.1*b*) be related to x without taking account of the effect of the non-homogeneous contributions under the integral of (4.1). Yet in the spirit of (3.1) we can conclude from figure 8(*b*) that the inner-layer developments mirror mainly the behaviour of the strongest component, the still-evolving u_{TS} field; on the other hand, the outer-layer behaviour characterizes primarily the local adjustment to the locally stronger forcing field $u'_{\mathrm{f}}(x, 11\ \mathrm{mm})$.

Generally, measurements of u'_{TS} of pure normal modes away from regions of forcing but in the presence of noise exhibit an inner u' maximum, then a rather sharp minimum beyond 0.6δ where ϕ_{TS} changes rapidly by π, followed by a shallow outer maximum, which extends beyond the edge of the steady boundary layer. Theoretically the locations of these maxima and the minimum depend on the frequency and the

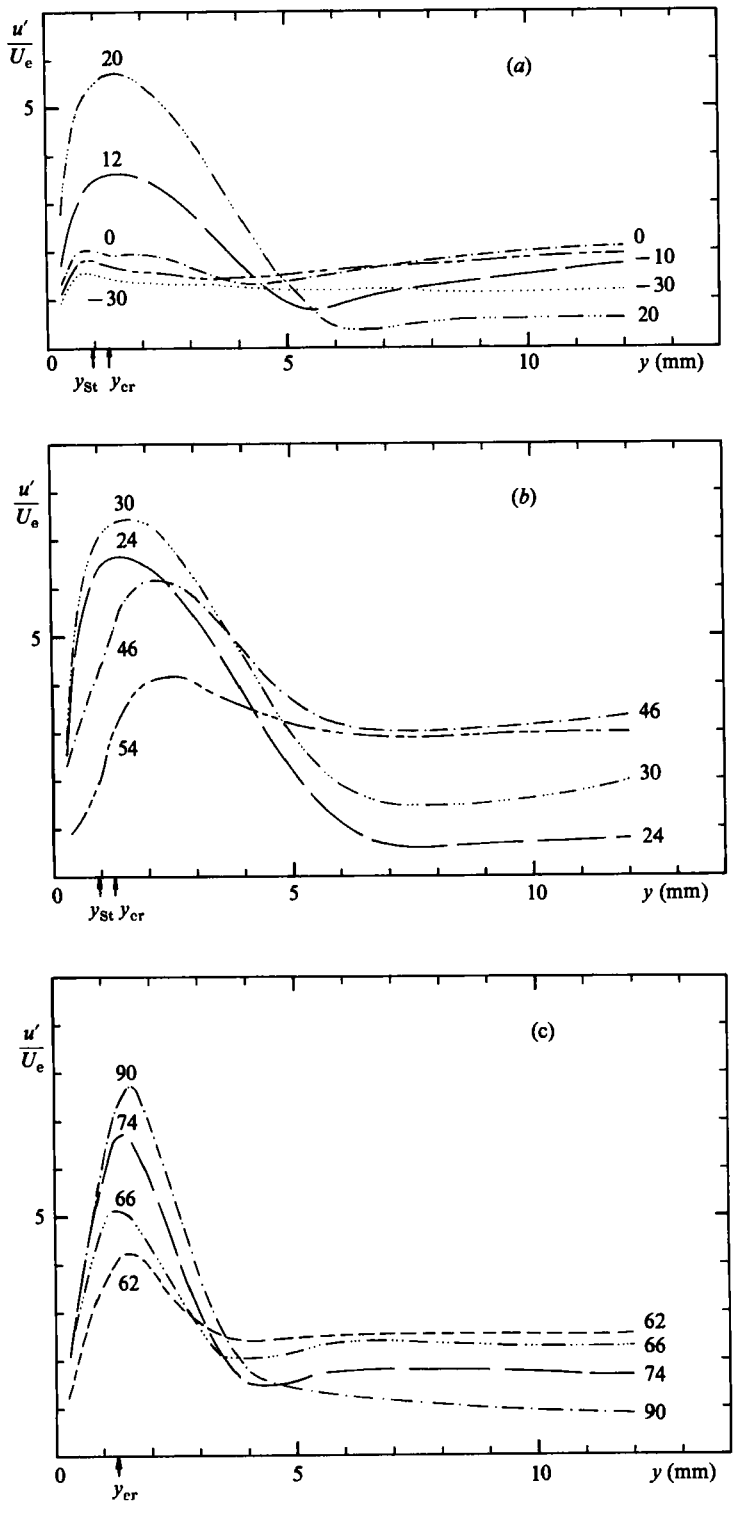

FIGURE 8(a–c). For caption see facing page.

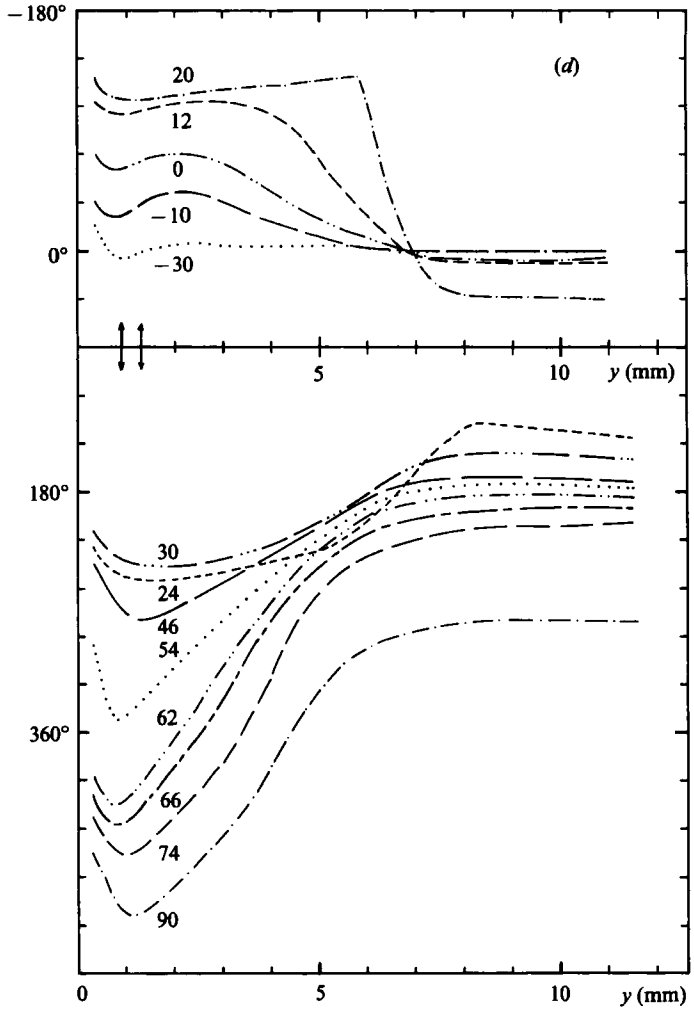

FIGURE 8. (*a*), (*b*), (*c*) Development in x (in mm) of $u'(y)$ and (*d*) of $\phi(y)$ for the unstable case U: $F = 0.53 \times 10^{-6}$, $\delta^* = 2.3$ mm, $Re_{\delta^*} = 1120$, Stokes overshoot $y_{St} = 0.96$ mm; for two-dimensional waves $\lambda = 78$ mm, $c_r = 0.32 U_e$.

Reynolds number, see e.g. figure 2 of Hama, Williams & Fasel (1980). When the u'_f forcing field is superposed, the y-minimum in the total signal $u'(y)$ is likely to degenerate to a local dip, in accordance with (3.1*c*); the associated 180° sharp change in ϕ_{TS} should be spread over a wider y-range. Both of these characteristics are observed in the region downstream of CC′. In figure 8(*d*), changes in total phase ϕ exceeding π take place over Δy of about 3.5 mm (i.e. 0.5δ) for $62 < x < 90$. Also, all the profiles in figure 8(*c*) (except one of the profiles at $x = 90$) show at least a hint of a dip in $u'(y)$ past the inner maximum. Furthermore, the smoothed average phase change for $1.2 < y < 3.6$ and $54 < x < 90$ in figure 8(*d*) is approximately 4.4°/mm. The agreement of this $\partial\phi/\partial x$ average with the theoretical two-dimensional slope $\partial\phi_{TS}/\partial x = k_{TSr}$ for 30 Hz, 4.6°/mm, may be partly coincidental.

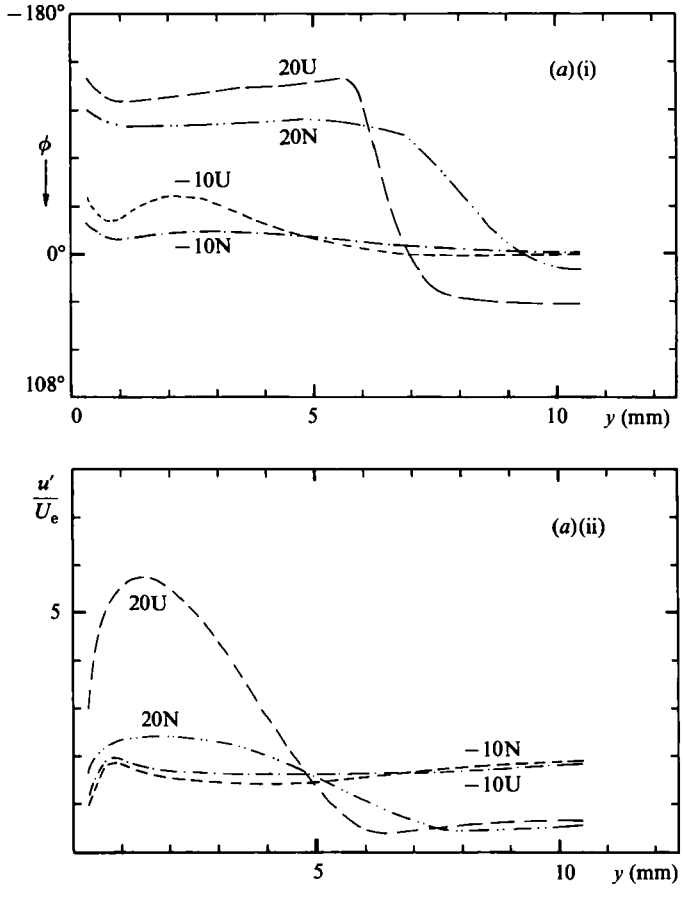

FIGURE 9(a). For caption see facing page.

4.4. *The slightly stable case N*

We recall the setting of the experiment: for the same source and shield geometry in figure 3 and the same mean velocity of 3.3 m/s and δ^* of 2.5 mm, case N differs from case S only in the forcing frequency, 30 Hz versus 50 Hz. At Re_{δ^*} of 550, the conditions correspond to the two-dimensional TS characteristics: $\lambda_{TS} \approx 46$ mm, $c_r \approx 0.40 U_e$, and $k_{TSi} \approx 0.0006$. This case, intermediate between cases S and U, was intended to test primarily the consistency with the trends and results already described. No features discordant with the concepts and response behaviour discussed in the preceding sections were observed. We shall therefore confine ourselves to illustrations of the more interesting facets of the increased but still damped response in regions AA′B′B and CC′D′D; see respectively figures 9(*a*)(i) and (ii) and 9(*b*)(i) and (ii).

Figures 9(*a*)(i) and (ii) disclose how case N partakes in the early phase advance and amplitude build-up discussed in detail in connection with figures 8(*a*, *d*). All three cases start with the Stokes-like profiles at the upstream sections. The subsequent relative amplitude development by $x = 20$ between u'_U and u'_N in figure 9(*a*)(ii) and u'_S in figure 7(*a*)(i) epitomizes the three responses U, N and S to the same initial stationary forcing field with positive $A(x)$ variations of figure 6. The broad growth across the inner layer, noted and discussed at its first appearance at $x = 0$ in figure

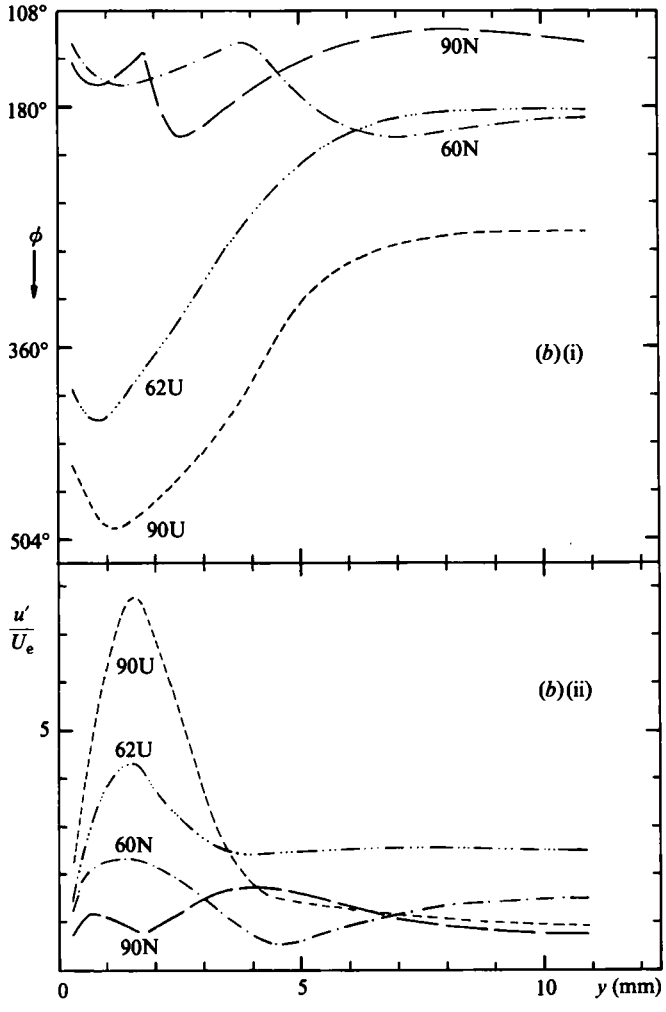

FIGURE 9. Comparison between the developments in the unstable case U and the just-stable case N: (*a*)(i) and (*a*)(ii) in the initial region AA′B′B of growth, and (*b*)(i) and (*b*)(ii) in the second region of growth CC′D′D.

8(*a*) for case U is certainly present at $x = 20$ for the case N. According to the conceptual equation (4.1), there can be net growth in x due to the local inhomogeneous increments $\Delta u_{\mathrm{TS}}(x')$ even when the factor $\exp\{-k_{\mathrm{TSi}}(x-x')\}$ is somewhat less than unity. When damping is too large, there are no local build-ups and the profiles up to $y \approx 4$ remain Stokes-like as in the u'_{S} behaviour in figures 7(*a*)(i) and (ii).

In the region of negative forcing interference BB′C′C, the N profiles subsided similarly to the U profiles in figure 8(*b*), but at lower levels. Interesting and contrasting behaviour took place in region CC′D′D; it is illustrated in figures 9(*b*)(i) and (ii) with the U profiles for counterpoint. As the inhomogeneous contributions decreased past $x = 60$, u'_{N} profiles declined in unusual lumpy patterns associated with sharp changes in $\partial\phi_{\mathrm{N}}/\partial y$. By $x = 140$ the profile declined further into an essentially low-level Stokes-like profile with a remaining local $\partial\phi/\partial y$ change at $y = 5.8$ mm. We have no substantiable explanation for this phase behaviour. Whatever the detail

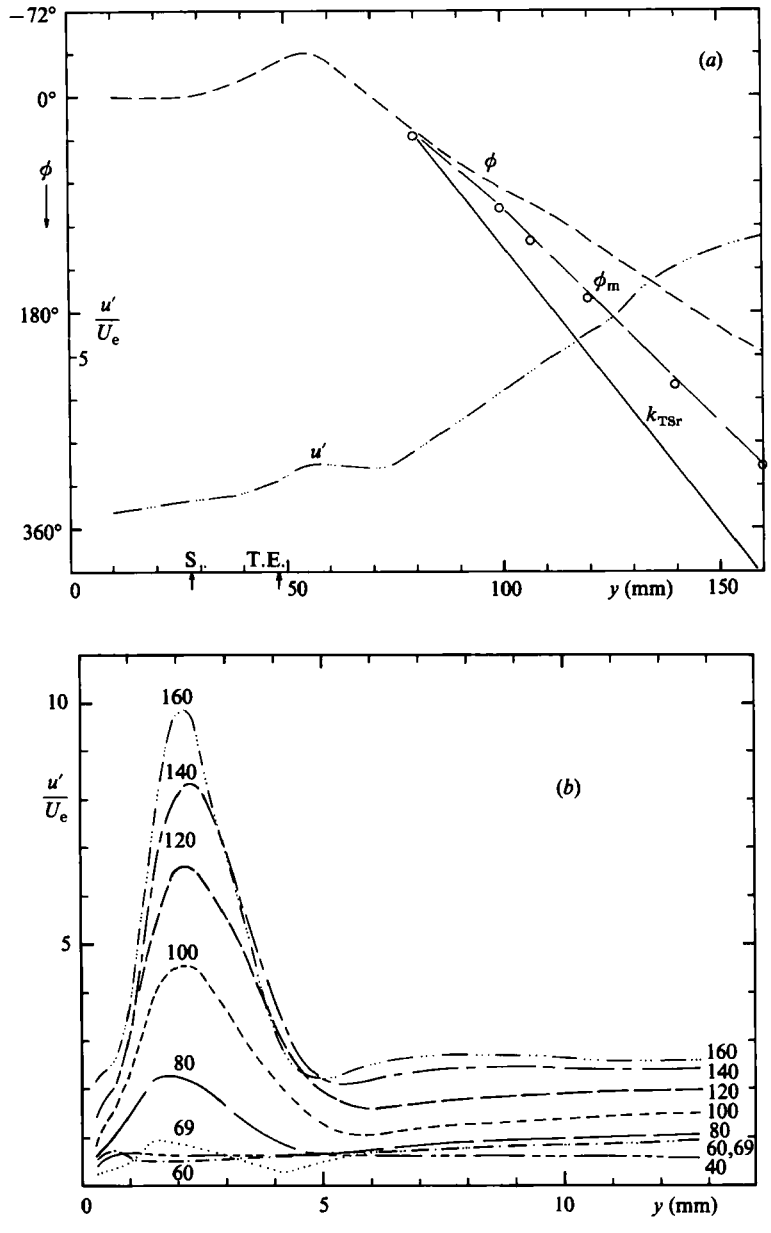

FIGURE 10(*a*,*b*). For caption see facing page.

causes, the main observation is that a slightly stable boundary layer can build up local fluctuation levels exceeding the excitation level. As the x-variation $A(x)$ of the causative unsteady pressure gradient subsides, so does the response level.

4.5. *The unstable case* U_w *with in-phase forcing field*

In its upstream position $-53 < x < 48$, the shielding plate under the source blocked the π change near $x = 22$ in the forcing phase $\phi(x)$ of figure 6 and generated the new forcing fields along $y = 11$ mm in figure 10(*a*). The corresponding total fields, $\phi(x, y)$ and $u' = u'_f + u'_d + u'_{TS}$ are presented in figures 10(*b*) and 10(*c*) respectively. Upstream

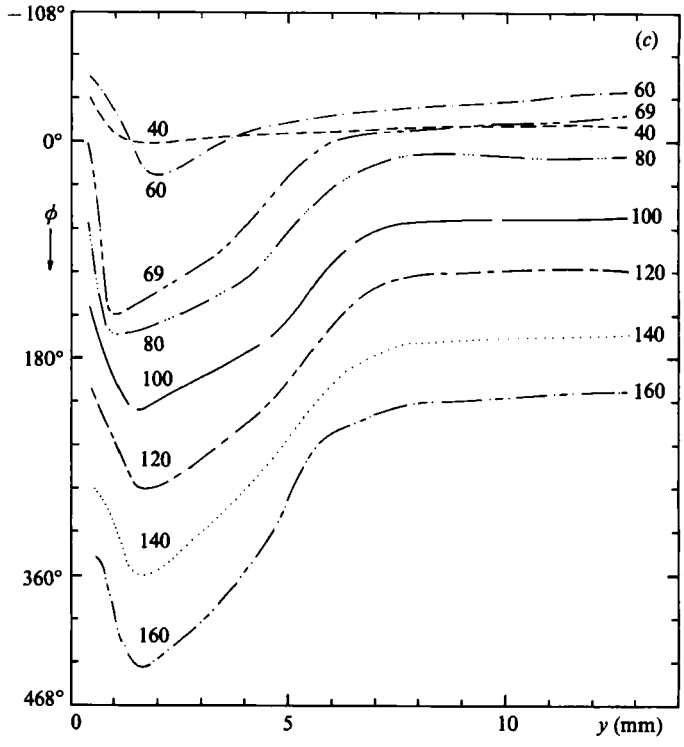

FIGURE 10. (*a*) Measured centreplane behaviour of the forcing field $u'_f(x, 11\text{ mm})$ and $\phi_f(x, 11\text{ mm})$ for the unstable case U_w with trailing edge of shield plate at $x = 48$ mm; ϕ_m measured phase at y-maxima of u'. (*b*) and (*c*) x-development of $u'(y)$ and $\phi(y)$ for case U_w.

of the plate trailing edge at $x = 48$, the initial profiles such as that at $x = 40$ are again Stokes-like, in agreement with expectations and the other experiments. At $x = 69$ unmistakable TS-like characteristics emerge as they did in u'_U at $x = 0$ in figure 8(*d*). The discussion of the latter and (4.1) apply here without modifications. Of importance is the fact that the TS-like development continues monotonically through the rest of the investigated range. The contrast between this monotonic growth and the reversal of the early trend experienced by u'_U in figure 8(*b*), corresponding to region BB′C′C, substantiates our discussion of the role of the forcing amplitude gradient $A(x)$. When the forcing 180° phase change is removed so is the negative interference and the associated ineffectiveness in TS-wave generation. (These findings have implications for optimal shaping of $A(x)$, should it be of interest in applications.)

It would be desirable to relate the growth of the maxima u'_m to the sources of the pressure fluctuations. The steady rise of the composite forcing function $u'_f(x, 11\text{ mm})$ implies that (i) the wake contributions must grow rapidly enough in x to compensate for the decaying contribution of the fixed three-dimensional source at $x = 28$, $y = 42$, and (ii) increments Δu_{TS} generated by the continued forcing are likely to strengthen the TS fluctuations throughout the region. The significance of observation (ii) becomes clearer when we compute the theoretical two-dimensional normal-mode growth from $x = 60$ to 160. Since the spatial amplification rate $-k_{TSi}\delta^*$ for case U_w is approximately 0.0028, the growth factor $u'_{TS}(160)/u'_{TS}(60) = \exp(-k_{TSi}x)$ over the 100 mm, i.e. $1.28\lambda_{TS}$, is only 1.13. The experimental ratio $u'_m(160)/u'_m(60)$ is

approximately 16 and the associated exponential rate is 22.7 times the theorctical $-k_{\mathrm{TSi}}$! This comparison reveals the key receptivity role of the cumulating inhomogeneous contributions in the integral of (4.1). The growth rates in the cumulative ranges of case U, corresponding to figures 8(*a*, *c*) also vastly exceed $-k_{\mathrm{TSi}}$. Furthermore, in the region of negative cumulation and rapid decay rates, in figure 8(*b*), the normal-mode growth rate $-k_{\mathrm{TSi}}\delta^* = 0.0028$ remains positive.

In the conceptual equation (4.1), the terms u_{TS} and Δu_{TS} are complex and functionally dependent on the forcing function $A(x)$ and its derivative, as well as on the TS eigenvalues. Consequently, the slope $\partial\phi_{\mathrm{TS}}/\partial x$ in a region of forced stimulation, $\Delta u_{\mathrm{TS}} \neq 0$, may have little relation to k_{TSr}, its value beyond the seeding region. It is therefore of interest to single out in this stimulation region the measured ϕ for the total signal at y-locations where the u_{TS} component is expected to be the largest, namely at the maxima u'_{m} in figure 10(*b*). These phases $\phi_{\mathrm{m}}(x)$ are shown as circles in figure 10(*a*); they were advanced by 120° so as to fit the figure. For purposes of comparison, the solid line through the leading point indicates the theoretical two-dimensional $\phi_{\mathrm{TS}} = k_{\mathrm{TSr}}x + \phi_{\mathrm{TS0}}$. The practically constant rate of measured phase lag from 100 to 160 makes it tempting to infer a wavelength, namely λ_{m} of 98 mm, and to attempt to relate it to the dominant forcing characteristics. The effort might be more justifiable if an asymptotic behaviour were extractable from the superposition equations (3.1).

Whatever the interpretations of finer features of the data, one overall aspect of the information in figures 10(*a–c*) is worth stressing. A substantial part of the observed growth could not have occurred without wake contributions to the increments Δu_{TS}. In §2.4 it was shown that the input equations (2.9) and (2.10) can be generalized to TS excitation by moving external pressure gradients. If the 'local' Fourier transform, ΔA_{Fw}, of the amplitude of the gradients $A_{\mathrm{w}}(x)$, has a non-vanishing contribution at the relative wavenumber $k_{\mathrm{TSr}} - k_{\mathrm{wr}}$, x-averages of forced inputs into the growth of TS enstrophy $\overline{\zeta_{\mathrm{TS}}^2}$ do not vanish. While these assertions are not verified here quantitatively, effective generation of TS waves by moving wave sources was demonstrated in this experiment, albeit in the presence of a stationary pressure source. Sections 2.2 and 2.3 document, unambiguously for the region up to BB′, that a stationary forcing field with variable $A(x)$ does generate TS waves. Now, in the region beyond the trailing edge of the shield plate, efficient TS generation, without reversal of growth rate, is observed in the presence of a stationary *and* a moving source field. Neither of these fields matches the propagation speed of the TS waves, a condition occasionally proposed as necessary for transfer of energy between linear waves. It is now apparent that the matching of characteristic lengths is the correct condition; this can be effected through the x-variation of the forcing pressure gradient whether the source is moving or stationary.

A final comment on the rapid growth of u_{TS} in figure 10(*b*) is in order. It has become customary to assume (*a*) that all the inhomogeneous receptivity seeding takes place upstream of branch I of the neutral curve, and (*b*) that the seeded TS wave packets amplify with the normal-mode rate beyond the neutral curve. The present experiments and those of Aizin & Polyakov (1979) (illustrated here in figure 1 and discussed further in the Appendix) demonstrate beyond doubt that growths far exceeding $\exp(-k_{\mathrm{TSi}}x)$ can occur within the TS instability loop as a result of unsteady pressure gradients. Scattered partial evidence suggests that growth rates exceeding the normal-mode rates also occur in receptivity to free-stream turbulence, Corke, Bar Sever & Morkovin (1986). Increased caution seems in order when using assumptions (*a*) and (*b*) in predicting boundary-layer behaviour in sensitive design applications. Evidently a homogeneous solution with initial conditions at branch I can be

overtaken by faster cumulative growth from local inhomogeneous sources beyond branch I, as symbolized by (4.1) with $x_0 = x_{cr}$.

In fact, the scheme for TS control of Liepmann, Brown & Nosenchuck (1982) by a periodically heated film at the wall operates on this principle. First the amplitude and phase of upstream-seeded TS waves, which grow 'naturally' in the boundary layer, are detected. Then forced wall vorticity waves are tailored by the hot film in such a way that the cumulative term in (4.1) has the same amplitude and opposite phase of the homogeneous solution from upstream. The local growth rate of the added TS component must of course substantially exceed the local rate $-k_{TSi}$ for the successful operation of the device. In receptivity to wall heating, the role of the crucial variable amplitude $A(x)$ of the unsteady pressure gradient is taken over by the amplitude $A(x)$ of the periodic term $-(1/\rho)(\mathrm{d}\mu/\mathrm{d}T)(\partial T/\partial y)(\partial u/\partial y)$ at the wall, where μ is the viscosity of the medium; in unsteady wall heating this term replaces the unsteady pressure gradient in the no-slip boundary condition (2.1) which determines the strength of the forced vorticity sources at the wall. Here the forcing field is dominated by the vorticity field at the wall with negligible v_f and p_f, so that the inhomogeneous input $\overline{v_f \zeta_{TS}}\, U''$ in (2.6) and (2.10) is absent. (Strictly speaking, the system of differential equations should include the thermal field; if the average heating rate over the film is small, the changes in the mean velocity field should be of higher order and confined to the proximity of the film.)

5. Comparisons, comments and conclusions

The detail discussion of the response fields in our four experiments in §4 uncovered no inconsistencies with the views on forced inputs developed in §§2.1–2.4. The response fields grow with $A(x)$ and decrease when $A(x)$ in effect changes sign as in region BB'C'C in figure 6, both at rates far exceeding $-k_{TSi}$. Furthermore, there is inferential evidence of vorticity increments at the wall and of velocity increments $\Delta u_{TS}(x, y)$ with a maximum beyond y_{cr}. Thus there is basic qualitative consistency. Inputs into $\mathrm{d}\overline{\zeta_{TS}^2}/\mathrm{d}x$ are not directly measurable; therefore the relations (2.9) and (2.10) involving the local Fourier transform of $A(x)$, $\Delta A_F(k_{TS})$ are not verifiable as such. The heuristic arguments in §2, while quite general, cannot lead to an actual seeding density $\Delta u_{TS}(x)$ that could be compared directly with the data. For that, a rigorous general solution of the full non-homogeneous problem is required. There seems to be no reason why, for a specific forcing field characterized by a particular $A(x)$, approaches like that illustrated by Reshotko (1984, pp. 4–5) or the Green function technique of Tam (1981) should not be successful.

The details of the evolution of the vorticity field in Fasel's (1976) numerical experiment gave further support to our view of the two inputs from the forcing non-homogeneous solution, especially of the role of the v_f component. But, to what extent is our viewpoint consistent with the receptivity experiments described in the book by Kachanov, Kozlov and Levchenko (KKL 1982) and in other Soviet publications? And to what extent do the views on receptivity of the Novosibirsk group conflict with the present experiments and interpretation? These questions call first for a brief resume of the largely unavailable Soviet work on receptivity.

5.1. *Views of Soviet experimenters on receptivity to pressure oscillations and vibrations*

Selected outlines of the experience of the Novosibirsk group were presented in Kachanov, Kozlov & Levchenko (1978) (hereinafter KKL 1978), Kachanov *et al.* (1979), Dovgal *et al.* (1979), Polyakov (1979) and in KKL (1982). Of these, the first

three are now available in English, and a copy of at least the first should be in the personal library of serious students of transition. Except for the book by Ginevskii *et al.* (1978) the other Soviet references discussed here deal with specific receptivity situations.

Early Soviet views on acoustic excitation of instability and transition were blurred by some experiments at high decibel levels which included a number of nonlinear receptivity paths. When nonlinear processes in the forcing field (including the speaker!) are excluded, the Soviet consensus is that TS instability processes are at work in dominant receptivity modes and that these are governed by the linearized Navier–Stokes equations. To sort out the experimental evidence, KKL (1982, p. 10) classify the active receptivity paths as (i) continuous or distributed, and (ii) localized or concentrated. In our terminology the localized paths comprise cases where the non-homogeneous contributions Δu_{TS} take place over a distance less than λ_{TS} long. KKL: 'By distributed generation we understand continuous distributed TS sources, spread over several λ_{TS}'. Category (ii) by definition includes: (*a*) the Aizin–Polyakov generation by irradiated roughness as in figure 1; (*b*) the TS generation by a vibrating ribbon inside of as well as in close proximity to a developed boundary layer; (*c*) the generation by vibrations of leading edges of two-dimensional bodies with radii of curvature r_c one or more orders of magnitude smaller than λ_{TS}; (*d*) the generation by far-field or near-field pressure oscillations with non-vanishing transverse velocity components v near such leading edges; (*e*) the generation by sound issuing from a small hole or slit from the surface under the boundary layer; (*f*) the generation by the periodically heated wall film with $l < \lambda_{TS}$ of Liepmann *et al.* (1982), etc. The first type of response of Polyakov *et al.* (1976) described in the Introduction would have to fall into the distributed category, and so would the axisymmetric sound-induced waves of Knapp & Roache (1968) over a smooth tangent ogive-cylinder body. The axisymmetric secant ogive body of Kegelman & Mueller (1986) probably falls into both classes, because there is a jump of 4.8° at the juncture between the ogive and the cylindrical body. Figure 11 of Kegelman & Mueller shows extended mean pressure gradients, signifying extended variations $A(x)$ of the forcing unsteady pressure gradient at 500–1000 Hz; also, according to a private communication from J. T. Kegelman, hot-wire traverses indicated the beginning of the superposition pattern *upstream* of the juncture. In our experiments with the sound source at $y_s = 42$ mm $= 6\delta$, $A(x)$ variations spread over $3\lambda_{TS}$ or more; the perturbation was compact enough to allow confident tracing of cause and effect and yet extended enough to exhibit negative interference in the cases where $A(x)$ in effect changed sign. In Fasel's (1976) numerical experiment, the forcing perturbation was prescribed over a length slightly less than $\frac{1}{2}\lambda_{TS}$ and falls therefore in the localized category (ii).

After 1975 KKL, impressed by the strong localized effects at the leading edge summarized below, looked almost exclusively to concentrated TS sources for explanation of receptivity experiments. In the 1982 book they point out that 'sharp changes in x of the disturbance amplitude excite in the boundary layer wave packets of diverse wavelengths, including those corresponding to TS waves'. Without considering specifics of the non-homogeneous inputs they state that the 'localized influences appear to represent greatly stronger TS excitation than distributed influences'. No distributed sources were investigated in any detail. The experiment of blunt-nose effects by Dovgal & Kozlov (1981*a*, *b*) unfortunately did not document the forcing amplitude variation $u_f'(x)$ outside the boundary layer.

5.2. *The issue of the leading-edge effects*

In face of general scepticism, KKL demonstrated to objective observers the nearly singular nature of TS formation associated with moderately sharp leading edges in classes (ii)(*c*) and (ii)(*d*), KKL (1975) and (1978) respectively. The conclusion of the untranslated 1975 paper was startling: in experiments on receptivity over flat plates, TS waves are induced by the vibrations of the leading edge rather than by the sound interaction with the boundary layer. The conclusion is well documented for the KKL 1 cm thick flat plate even in the presence of the relatively low dynamic pressure at the tunnel speed of 8.7 m/s. Is the conclusion equally valid for the sturdier, 2.5 cm plate of Polyakov *et al.* (1976) at 24 m/s and the viscoelastically damped 1.25 cm plate of Shapiro (1977) at 29 and 41 m/s?

In the experiments of Polyakov *et al.* (1976) an effective TS-wave origin near the leading edge is contraindicated by the growth of the first type, commencing halfway through the TS amplification region; to be induced at the leading edge the growths would have to start close to Re_{cr}. As mentioned in §1, the second type of response, originating upstream of the reach of their traverse, could be consistent with TS induction near the leading edge. Shapiro reported a vibratory velocity of the plate 'at test speed' as less than 0.015 mm/s at a sound level of 95 dB, i.e. at u'_{ac} of 3 mm/s. Gedney (1983) measured the TS response of the *same plate* to a 500 Hz sound excitation at 89 dB in presence of flow at 29 m/s. If this response had been dominated by the leading-edge vibration, Gedney would have needed only to still the leading edge to cancel the TS waves. Gedney, however, accomplished the cancellation by superposing an out-of-phase TS wave caused by vibrating the plate with a shaker so that the leading-edge amplitude was 29 mm/s, vastly exceeding the passive amplitude reported by Shapiro! Thus for this case there must be at least one additional effect. We could speculate as to the most likely source of this effect – presence of a weak v' component in the sound beamed at the leading edge from upstream, as KKL would suspect, or the thickness effect (which leads to a sharp local minimum of Shapiro's mean pressure coefficient of at least -0.06) as analysed by Goldstein (1984), etc. As noted in §1, the perennial need for speculation in receptivity experiments generally comes from inadequate definition of the forcing field, which in the leading-edge problems includes determination of the equivalent of $A_f(x)$ and $\phi_f(x)$ around the leading edge as well as up to the x station where the response is measured.

5.3. *The 1978 KKL experiments*

KKL (1978), in effect, provide the above information near the leading edge plus substantial details inside the boundary layer. Its significance goes beyond receptivity issues in its documentation of mean and periodic flow in the proximity of a relatively sharp leading edge and in its illumination of nearly singular asymmetric behaviour. Since fortunately it is available in English, we merely describe its most pertinent results and implications and supplement it with figure 11, important for reconciliation with our figures; figure 11 was left out of KKL (1978).

Classes (ii)(*c*) and (ii)(*d*) merge when one thinks in terms of the relative velocity between the fluid and the leading edge. KKL refer to thin-plunging-airfoil theory as a guide to the key effect: a large magnification relating v' to u' around the leading edge, which clarifies the high sensitivity to asymmetry and v'. In essence they probe the parameter regime where the inviscid-zero-thickness singularity is removed by small but finite radius in presence of viscosity. In their figure 2 with leading edge as origin they map out a mean-flow field with no apparent separation, a velocity

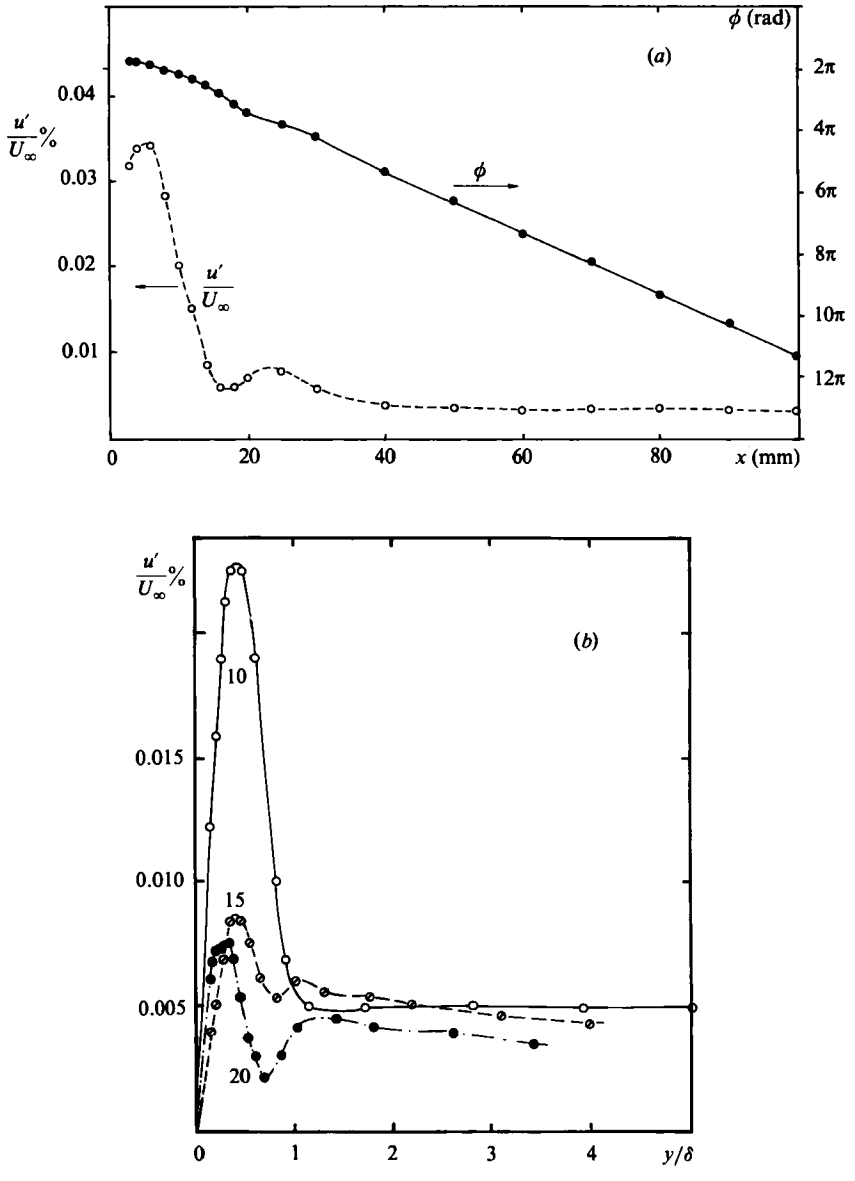

FIGURE 11 (*a*, *b*). For caption see facing page.

overshoot exceeding $1.07U_\infty$ near $x = 4$ mm, and a subsequent slow adverse pressure gradient. They speak of nearly quantitative verification of their unsteady measurements. The theory they refer to is due to Maksimov (1979) and Kachanov *et al.* (1979) and consists of difference solutions of linearized Navier–Stokes equations, with strong curvature effects bypassed through *ad hoc* assumptions. No asymptotic arguments in the r_c, ν and ω parameters are adduced for these assumptions. Linearity of the field is checked experimentally over a range of disturbance amplitudes.

Despite its appearance in their figures 2, 3 and 5, the KKL 10 mm thick plate is asymmetric with a 2:132 mm ellipse on the working top side and a 8:132 mm ellipse on the lower side of the nose. All figures and descriptions are for the upper surface

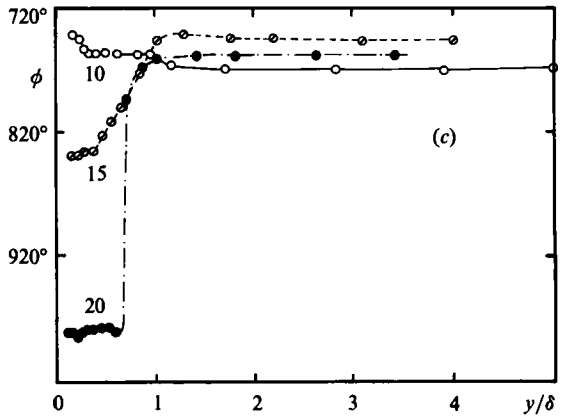

FIGURE 11. (*a*) Development in x of total signal u' and ϕ at height $y(x)$ for which $U(y)/U_e = 0.5$ over the upper surface of a plate with small radius of curvature at leading edge at $x = 0$. Forcing field due to vertically vibrating horizontal ribbon at $y = -6.5$ mm upstream of the edge, with small normal velocity fluctuation v'_f approaching the nose. Critical Re near $x = 300$ mm. Kachanov *et al.* (1982). (*b*) and (*c*) Development in x (in mm) of profiles of total signals $u'(y)$ and $\phi(y)$ for the flow of (*a*).

of the plate. The amplitude isolines and the phase lines for these unsteady fields were mapped out in great detail for -10 mm $< x < 20$ mm. The fields were generated by a 3 mm wide, 0.1 mm thick ribbon vibrating in the y-direction at $y_r = -5.5$ mm and $y_r = 6.5$ mm in cases (*a*) and (*b*) and by the same ribbon rotated 90° to the flow and vibrating in the x-direction in case (*c*). The ribbon, at an unspecified x_r upstream of the leading edge, generated a fixed dipole field and wake quadrupole fields travelling at $U_\infty \pm 3\,\%$; only the outer potential undulations of the wake reached the surface of the plate in the region of interest. In case (*a*), with a flow attachment point on the lower surface, the small oscillatory v' component at the nose was associated with a prominent frequency-dependent local maximum of u' at about $x = -0.13$, $y = 0.4$; a hot-wire traverse at $y = 0.5$ indicated a 90° rise and fall of the phase, independent of frequency, in the 2.5 mm of travel across this formation. Evidently, unsteady vorticity accumulates periodically in this region, without physically shedding; instead, a perturbation wave propagates downstream in the upper boundary layer, a wave which KKL identify as a damped TS wave.

An unpublished figure shows that in case (*b*), with flow attachment on the upper working surface, the same vortical formation has a very small local maximum with a 90° fall and rise along the $y = 0.5$ traverse, and farther downstream a weak wave propagating with U_∞ in the upper boundary layer. In our terminology the wave corresponds to the u'_f field of the locally dominant forcing wake and its Stokes layer, with any damped TS wave too small to be evident in the total u' and ϕ measurements. (In a new figure extending past $x = 300$ and Re_{cr}, the remnants of this small u'_{TS} or new distributed contributions to u'_{TS} by the continued but weaker wake forcing are seen to amplify – see figure 4 of Dovgal *et al.* 1979.) The horizontal oscillations in case (*c*) were intended to underscore the v-role by near-cancellation of the v-fluctuations at the leading edge. As KKL anticipated, the u' peak was replaced by a *decrease* in u' fluctuations as $x = 0$ was approached and rapid phase changes were absent; again there is a weak wave propagating with U_∞ in the upper boundary layer, essentially the forcing wake field and its Stokes layer.

In figure 11 we present the early developments of u' and ϕ in the upper boundary layer for the key case (*a*), a figure left out of KKL (1978). The x-traverse in figure 11(*a*) was taken along a path with constant mean velocity $U(y)/U_e = 0.5$. There is a $u'_{\min}$ at $x = 2.5$ not emphasized in figure 11(*a*), a maximum at $x = 5.5$, followed by a sharp drop with another pair of extrema near $x = 20$. Clearly this is the compact region of active generation of unsteady vorticity, with possible negative interference past $x = 5.5$. The external $u'_f(x, 3\delta)$ in figure 11(*b*) and the slow change in $\phi_f(x, 3\delta)$ in 11(*c*) indicate that this region is shielded from the wake and the forcing field is dominated by the stationary dipole. The y-profiles at $x = 20$ in figures 11(*b*, *c*) look like a superposition of the dipole forcing with a TS wave according to equation (3.1). Unfortunately, there is no information on $u_f(x, y > \delta)$ past $x = 20$ to indicate the rate of decay of the dipole field, which may be slower than the TS decay at these low Reynolds numbers. KKL (1982, p. 16) assume that the u' value in figure 11(*a*) consists of a pure damped TS wave. They comment that the measured decrease by a factor of 1.33 between $x = 40$ and 100 is very much smaller than the 8.2 decay factor expected of the TS wave in a nominal Blasius layer. Perhaps this one clear inconsistency is explainable by a combination of (i) the presence of slowly falling non-zero u'_f in the total u' curve in figure 11(*a*) and (ii) by true slower TS decay in this region of slightly inflected mean velocity profiles; downstream of the aforementioned mean velocity overshoot at $x = 4$ there is an adverse pressure gradient in which 15% or more of the dynamic pressure is slowly recovered. As a consequence of (i) the slope $\partial\phi/\partial x$ in figure 11(*a*) differs from k_{TSr} because of the presence of the variable ratio $p(x, y) = u'_f(x, y)/u'_{TS}(x, y)$ in (3.1*b*); the tempting simple inference from figure 11(*b*) of $\lambda_{TS} = 20$ mm is likely to be incorrect.

We are unaware of comparable information on steady and unsteady leading-edge effects. Although independent confirmation is always desirable, there is little doubt that the geometry in the mathematical models of Goldstein (1983), Murdock (1980), and Tam (1981) is over-idealized and governed by different, second-order receptivity paths. Furthermore, the experiments of Shapiro (1977) and Gedney (1983) discussed in §5.2 must be affected, if not dominated, by leading-edge effects. Clearly the effects of unsteady relative motion at sharper leading edges are powerful and the induced TS waves can survive the damping upstream of Re_{cr}; in real geometries that damping is much milder than estimated by Murdock because of the inevitable adverse pressure gradients associated with the strength-dictated thickness of the models.

5.4. *Final comparisons*

Dovgal, Kozlov and Levchenko (1980) also placed their vibrating ribbon in the free stream at $x_r = 251$ mm, $y_r = 9$ mm $\approx 2.2\delta$ above the KKL (1978) plate, sufficiently far downstream of the adverse pressure gradient. At $U_e = 5.8$ m/s and $\delta^* = 1.43$ mm, the critical Re_{δ^*} for the vibration frequency of 73 Hz occurred somewhat upstream of x_r. Indeed, the measured $u'(y)$ profiles already disclosed at $x = 260$ substantial u'_d and u'_{TS} responses to this forcing field of a fixed doublet and superposed convected wake quadrupoles. Comparisons were made with the response for the case when the ribbon was moved to $y_r = 0.15$ mm, deep in the boundary layer. The significance of the differences, though not negligible, were discounted without mentioning the question of the strength of the probably laminar wake contributions. Weak wake effects would have been more discernible on phase maps, but in contrast to the 1978 paper, none were offered or discussed. It is a pity that this information and the definition of the forcing fields through $u'_f(x, y_0)$ and $\phi_f(x, y_0)$ with y_0 above the boundary layer for $x > 200$ are not available; it would probably show that the doublet excitation field extends over several λ_{TS}. Except for accessibility problems

near the ribbon location, the configuration had some advantages over that in our experiments: (i) the field is quasi-two-dimensional and (ii) the wake induction is probably milder. In our case the wake radiation was from transitional and early turbulent wakes modulated by the primary sound source at the test frequency. The doublet also has a phase reversal under the ribbon. Hence there should be a region of negative interference as in our experiments.

Experiments by Dovgal & Kozlov (1981*a*, *b*) on blunt bodies exposed to sound (where distributed TS sources are probably important) also suffered from the absence of documentation of the non-constant forcing fields $u_f'(x, y_0)$ and $\phi_f(x, y_0)$ just outside the boundary layer. The experiments are very interesting for the observed patterns of behaviour with shape and frequency, but unfortunately they do not provide the data to connect cause and effect quantitatively. In the first paper sound was beamed from the downstream diffusor axially onto two axisymmetric cylinders, 2 in. in diameter; one had a hemispherical nose and the other had its frontal outer rim profiled as an elliptical quadrant with the streamwise semi-axis of 25 mm and the radial semi-axis of 8.4 mm. The inferential conclusions of Dovgal & Kozlov are rather vague: 'Probably the generation of TS waves takes place throughout the region of the adverse pressure gradients; nevertheless the sound interacts most effectively with the boundary layer in the neighbourhood of the nose'. These adverse mean pressure gradients extended beyond $x = 100$, a distance of 5–12 observed λ_{TS} at frequencies from 97 to 273 Hz. For the elliptically rounded rim, there is evidence (their figure 3) of Δu_{TS} contributions at $x = 10$, where the boundary layer undoubtedly is still stable, in qualitative agreement with our view. In the second paper interesting effects of sound beamed from downstream onto a 14% thick symmetric airfoil were investigated, but again the variable forcing field, diffracting and scattering around the airfoil, was not measured. The u_{TS} response spread over 6–$8\lambda_{TS}$ before its final rapid TS amplification by the inflected profiles in the decelerating boundary layer as it approached laminar separation. In this downstream region a measure of control over mean profiles and separation was exercised by the sound-induced, overgrown vorticity waves. There were no apparent inconsistencies with our concepts of non-homogeneous input and response.

The Knapp–Roache (1968) largely visual evidence of acoustical TS-wave stimulation over an axisymmetric tangent ogive-cylinder body has been a long-standing reminder of the efficacy of sound-induced distributed TS sources. The nearly singular effects due to relative v motion at the sharp nose (such as described in §§5.2 and 5.3 for two-dimensional models) could not seed the observed *axisymmetric* TS waves; furthermore there were no other concentrated sources since both the mean pressure gradient and the acoustic pressure gradient evolved smoothly at the cylinder juncture. However, neither this experiment nor its more quantitative 1986 follow-up in the same wind tunnel by Kegelman & Mueller provides more than qualitative support for our concepts. Besides the lack of adequate definition of $u_f'(x, y_0)$ and $\phi_f(x, y_0)$ at the edge of the boundary layer, the variation in the instability parameters of the boundary layer itself presents a difficult obstacle to quantitative evaluation. This is illustrated and discussed by Kegelman & Mueller in connection with their figure 12, which displays widely different neutral curves for three x-stations only three 'natural' λ_{TS} apart. Although receptivity theory will ultimately be applicable to bodies with variable thickness, in explorative experiments the variations in the TS amplification characteristics complicates almost critically the task of tracing cause and effect quantitatively. These considerations and the awareness of the leading-edge effects were primary in our 1981 decisions on the experimental geometry in figure 3 where both features are absent.

5.5. *Toward a unified view of receptivity experiments*

Of the more rcliable and revealing receptivity experiments reviewed in §§5.1–5.4 and in the Appendix, two experimental configurations are not adequatcly covered by the concepts of §§2.1–2.4. The first is the KKL (1978) leading-edge configuration of §5.3. Although the no-slip condition (2.1) undoubtedly governs the unsteady wall-vorticity sources near and around thc leading-edge, the very definition of TS characteristics in the region presents a major problem. Furthermorc, the sharp curvature may be responsible for additional effects. Figure 11 suggests that the concepts may be applicable in principle from some small distance on, say from $x \sim 4r_c$.

The second exceptional configuration is that of Aizin & Polyakov (1979); the case is discussed in the Appendix and illustrated in figure 1. Here our reliance on the no-slip condition at a flat wall is spoiled by the change in the boundary itself, albeit very small. The boundary information is not contained in our input-controlling function, the amplitude $A(x)$ of the unsteady pressure gradient beyond thc boundary layer. Nor does it arise from first principles as the wall boundary condition for the periodically heated strip of Liepmann *et al.* (1982) (see end of §4.5). However, the Aizin–Polyakov effect undoubtedly gencrates a non-uniform distribution of vorticity sources at the wall and over the mylar strip and should be enhanced by the $v_f(x)$ motion induced near the edges of the strip, in agreement with our general view. As indicated by Goldstein (1985), such local information at protuberance Reynolds numbers on the order of unity should reside at the lowest deck of the boundary layer. Once the effective $(\partial\zeta/\partial y)_f$ and v_f disturbances arc introduced, the stage is set for the TS self-excitation loop to take over.

The Aizin–Polyakov configuration constitutes a concrete example of a new 'covert' class of geometrically enhanced receptivities which may not be traceable to changes in commonly measured mean profiles. In principle, there is an effect on the mean velocity profiles due to the extra-thin A-K mylar strips and their mysterious 'technical' juncture (see the Appendix). In practice, the resolution of the instruments, near-wall instrument interference, and omnipresent scatter invariably hide such weak evidence. Yet in the presence of acoustic irradiation, the Aizin–Polyakov experiments document receptivity significantly larger than that of the smooth-wall configuration. Recent experiments (Corke *et al.* 1986), demonstrated growth of TS waves in boundary layers with moderate distributed roughness far in excess of $-k_{TSi}$ based on measured mean velocity profiles. The overall evidence suggests strongly that the most likely cause of this extra growth is roughness-enhanced receptivity to free-stream disturbances, including irregular low-frequency pressure fluctuations. The enhanced receptivity to sound of isolated roughness elements large enough to cause local separation is known and qualitatively understood: strong unsteady vorticity sources around the separation line are followed immediately by strong inflectional amplification over the separated regions. This is, of course, the basic mechanism of boundary-layer tripping devices, but in such cases, the distortion of the mean profile is measurable. The special enhanced-receptivity aspect of the A-K effect calls for careful explorations of the full neighbourhood of the low-Reynolds-number strips by hot-wire anemometer or LDV.

Besides the distinct phenomenological fields at the leading edge and at the thin mylar strips, the experiments at Novosibirsk describe a number of specific receptivity fields which appear fully consistent with the concepts of §2. The Dovgal–Kozlov experiments on blunt noses further bear out our observation that the thickness distribution of bodies brings out automatically a variation of the amplitude $A(x)$ of

the acoustic pressure gradients which spawns TS waves. This fact makes the $A(x)$ mechanism almost omnipresent. Their evidence of extensive interference patterns between u_f and Δu_{TS} demonstrates again that the non-homogeneous Δu_{TS} cumulation in (4.1) is not directly dependent on k_{TSi}; unmistakable cumulations are evident on all the blunt noses in the region of positive k_{TSi} upstream of Re_{cr}, wherever there is significant $A(x)$ variation. The variety of the Soviet experiments with speakers and vibrating ribbons further indicates that receptivity does not distinguish between acoustic and 'incompressible' unsteady pressure gradients or between far field and near field, in consonance with the controlling no-slip condition (2.1). The valid Soviet distinction between distributed and localized sources of TS induction cleared away confusing interpretations of early experiments but did not address the issue of the decomposition of the total measured field into all the conceptually identifiable constituents nor the deeper issue of the nature of the mechanisms of receptivity.

Mungur (1977) and unpublished work by M. Gaster (1972) looked for the key to acoustic receptivity by decomposing the total field into irrotational forcing velocity fields and divergence-free velocity response fields. There are some difficulties in this approach – the TS response field, after all, has an irrotational component which extends beyond δ. However, both authors identified a probable forced contribution to u_{TS} as the non-homogeneous field term $v_f U'$ in the x-momentum equation without considering what conditions prevent its cumulative effect from vanishing. The term is equivalent to our $v_f U''$ contribution to ζ_{TS}; the condition for its non-vanishing contribution to $\mathrm{d}\overline{\zeta_{TS}^2}/\mathrm{d}x$ is equation (2.10). The corresponding early build-up of the vorticity field away from the wall is clearly distinguishable in Fasel's (1976) numerical experiment. In the case U experiment in §4.3 the equivalent non-diffusive forced growth of u'_{TS} is observed beyond y_{cr} at $x = 0$ in figure 8(*a*); in case U_w it emerges at $x = 69$ in figure 10(*b*).

The mechanism is, of course, operative for some distance upstream of these two sections, where $A(x)$ varies but u'_{TS} remains obscured by noise and the large u'_f component of the measured signal. Upstream of the sections with such clear evidence of the incipient Δu_{TS} response the measured fields are Stokes-like, in accordance with the theory of §2.1. The upstream Stokes-like profiles appear in all our experiments – see figures 7(*a*)(i), 7(*b*)(i), 8(*a*, *d*), 9(*a*)(i) and (ii) and 10(*b*, *c*). No independent evidence for this feature has come from any other receptivity experiments. It is also of some significance that the incipient growth from the Stokes-like distributions due to non-homogeneous Δu_{TS} increments, can take place anywhere including in between the two branches of the neutral curve (as in the 1976 experiments of Polyakov *et al.* and in our cases U and U_w), and not only at the leading edge or at x_{cr}, as is occasionally implied.

According to (2.1) any unsteady, spatially varying pressure field beyond the boundary layer imprints vorticity sources in the lowest deck of the boundary layer in its own image. If these forced fluctuations near the wall do not average out to zero, this represents a clear input mechanism from external disturbances to the forced vorticity field in the boundary layer, not discussed by Mungur or Gaster. In essence, part of the reservoir of environmental disturbances outside the boundary layer is transferred directly to the vortical disturbances deep within the boundary layer; there the boundary-layer filter-amplifier can damp or enhance them. This basic seeding path cannot be avoided as such; however, its efficacy in harmonic excitation depends on $A(x)$.

The heuristic arguments at the end of §2.4 in connection with excitation due to wakes imply that the external forcing pressure field need not be stationary; in fact,

the propagation speed of the external field does not matter as long as the local Fourier transform of $A_w(x)$, $\Delta A_{wF}(k_{TSr} - k_{wr})$, does not vanish when evaluated at the difference wavenumber $k_{TSr} - k_{wr}$. The increments Δu_{TS} for higher x-values in the case U_w of §4.5, observable in figures 10(*b*, *c*), are caused primarily by such wake forcing. Hot-wire traverses indicated that the forcing wakes of the shield plate and of the piping to the pressure source in figure 3, as well as the convected fluid ejected periodically from the source orifices, were turbulent or transitional in cases U and U_w with forced $\exp(-i\omega t)$ acoustic modulation. Since the strength of the resultant travelling pressure fields depended on sensitive secondary aspects of the configuration, we considered the excited radiating wakes as a nuisance and did not attempt to map them in detail. However, the case U_w demonstrates that external quadrupoles travelling with phase speed $c_{wr} \neq c_{rTS}$ can definitely induce TS waves.

The implication of these findings is that this receptivity path probably exists for free-stream turbulence above the boundary layer y_δ even when it is not modulated at ω_{TS}. Active, i.e. non-frozen, larger-scale turbulent structures above y_δ transmit unsteady, x- and z-dependent v_{ft} and p_{ft} fields on their scales through the boundary layer to the wall. Under proper conditions, the non-uniformity of these forcing fields in x, z and t may lead to build-up of TS wave packets through processes equivalent to those in case U_w. That the averaged spatial growth of u'_{TS} could then exceed $-k_{TSi}$, as Kendall (1984) has observed, would not be surprising; as we have seen in case U_w in §4.5, the Δu_{TS} cumulation rate can be far larger than $-k_{TSi}$. The difficulty in modelling this receptivity path mathematically is in the representation of the forcing fields as *non-averaged* functions on which there is little information. While this receptivity path probably exists, there is no assurance that there are no other more efficient paths. In the preceding discussion the effect of the turbulent vortical field which is ingested into the boundary layer has been left out. There is scattered evidence that the turbulent disturbances ingested near the leading edge of axisymmetric bodies decay very rapidly near the wall. However, there is no information on the interaction between turbulent vorticity convected into the boundary layer near and past x_{cr} and the vorticity and shear of the boundary layer itself. Contributions Δu_{TS} from this interaction may or may not be more efficient than the generalized analogue of the U_w case.

A comment is in order concerning the practical problem of receptivity to elastic vibrations of the body surface away from the leading edge. In this non-homogeneous problem the forcing conditions are at the wall instead of beyond the boundary layer, and they are quite regular. For small vibrations the linearized boundary condition on v at the moving wall should be transferable to $y = 0$. The resulting pressure field is unknown and must be determined, possibly through triple-deck formulation. Physically, the role of the forcing p_f and v_f fields in the receptivity part of the problem should be qualitatively the same as in the receptivity paths examined earlier. A number of unexpected early transitions to turbulence in flight has been vaguely attributed to vibrations of the skin of the vehicle. Careful analytical treatment should identify the dangerous conditions and stimulate corroborating experiments. A report by Lemcke *et al.* (1970) on an international cooperative research effort in wind tunnels and in flight using the same physical model of the JARIBU hypersonic vehicle makes most instructive reading; a gross discrepancy between flight and laboratory transition Reynolds numbers was ultimately ascribed to disturbances due to skin vibrations induced by the rocket motor on the basis of circumstantial but plausible evidence.

The relevance of the present approach to boundary-layer receptivities to free-

stream turbulence, to wall vibrations, to local harmonic wall heating of Liepmann *et al.* (1982), etc., indicates that the choice of the variables comes close to the essence of the phenomena. The approach is really forced upon the experimenter when faced with interpretation of the measured total u' and ϕ-fields which the instruments cannot decompose into the forcing and response fields. The decomposition must rely therefore on the physico–mathematical properties of the superposed fields. The adoption of the $(\ )_f$, $(\ )_d$ and $(\ )_{TS}$ components has the advantage of paralleling the theory of forced linear systems. This immediately mandates the experimental definition of the forcing field by its values around the open domain, e.g. AA′B′C′D′D in figures 3 and 6. (Of all the receptivity experiments only KKL (1978) provided equivalent information.) The fact that along A′B′C′D′ the fields $(\ )_d$ and $(\ )_{TS}$ are dwarfed by $(\ )_f$ is very useful. The focus on vorticity is also fruitful because (*a*) the boundary condition $(1/\rho)\,\partial p/\partial x = \nu.\partial\zeta/\partial y$ shows how the external disturbance (albeit slightly modified by the passage through the sheared layer) forces a distribution of wall vorticity sources in its image, and (*b*) the vorticity of the forcing field is confined to the thin Stokes sublayer. Characteristic (*b*) makes possible the identification of the other transfer mechanism: the conversion at any point of mean boundary-layer vorticity U'' by the forcing unsteady transverse velocity field v_f into an increment in unsteady TS vorticity or, after multiplication by ζ_{TS} and averaging, into a contribution to the growth of TS enstrophy. These are, of course, heuristic arguments and should be verified by rigorous theory, possibly by techniques described by Reshotko (1984) and Tam (1981). Nevertheless, the overall concepts appear to unify rather successfully the interpretation of all the reliable experiments on receptivity to unsteady pressure gradients.

Since this paper was written some relevant papers have appeared in the literature, e.g. six papers in Kozlov (1985) and a review of the triple-deck approach to receptivity problems by Goldstein (1986).

The experiments reported here were conducted in 1981–82 while M. Nishioka visited the Illinois Institute of Technology. He wishes to acknowledge the assistance of the University of Osaka Prefecture, Osaka. The work was supported in part by the National Science Foundation through Grant MEA-8021942 and by the Army Research Office through Project P17690-E. Special thanks go to Michael Plesniak for his enthusiastic assistance with the experiments. The contribution of results of unpublished numerical experiments by Hermann Fasel to our model is gratefully acknowledged.

Appendix. The Aizin–Polyakov experiment on irradiated roughness

The rather intriguing experiment to which figure 1 refers (Aizin & Polyakov 1979) has appeared only as a publicly unavailable Russian 'preprint'; it is therefore desirable to describe briefly its contents. The 25 mm thick flat plate of Polyakov *et al.* (1976) was used, primarily at free-stream speed U_1 of 23.4 m/s. It had a composite elliptic nose (2:165 mm at upper surface, 23:69 mm at lower surface); at $x = 565$ mm the nose is said to have an otherwise unspecified 'technological juncture' with the main body of the plate, which extended to 3900 mm. The roughness in the form of extra-thin mylar strips 12 mm wide was affixed to the plate at $x = 565$, corresponding to $Re_{\delta^*} = 1550$; profilometer (!) measurements *in situ* indicated three operational thicknesses in mm: $H_1 = 0.012$–0.017, $H_2 = 0.020$–0.025, and $H_3 = 0.032$–0.037. With $\nu = 15.10^{-6}$ m^2/s, the inferred δ^* is 1.0 mm so that H/δ^* values are below 4 %.

These are exceedingly small roughnesses, immersed deep in the linear stress region of the Blasius profile; their local Reynolds number $Re_H = HU(H)/\nu$ is then given by the formula $Re_H = 0.57 Re_{\delta^*}(H/\delta^*)^2$. Re_H rises quadratically up to 1.05 for H_3. No inertial separation at the edges is expected for such low Re_H. The effects observed should be distinct from the known separation-controlled high sensitivity to sound for larger single roughnesses such as $H = 0.15\delta^*$, $Re_H = 20$, which was used in preliminary experiments by Aizin & Polyakov. The acoustic excitation at 138 Hz and 104 dB was beamed upstream along the plate from a speaker in a downstream diffusor. The resulting unsteady field in our figure 1 was measured with a DISA hot wire, traversing at an unspecified height y (or possibly at $u'_{\max}$) near and downstream of protuberance H_3.

That ratio of the u'_{TS} response in figure 1 to the excitation u'_{ac} is shown in their figure 3 to follow the same growth curve for excitations of 100, 104 and 108 dB, i.e. the experiments are in a linear regime. At Re_{δ^*} of 1550, the frequency of 138 Hz corresponds to dimensionless $F = 2\pi f\nu/U_1^2 = 24.10^{-6}$ and a TS wavelength of 50 mm. The strips with a width of $0.24\lambda_{\mathrm{TS}}$ represent very local wall-geometry perturbations ending physically at x_1. A coefficient of generation or receptivity, k_{13}, is defined as the ratio of $u'_{\mathrm{TS}}/u'_{\mathrm{ac}}$ at x_1; u'_{TS} at x_1 was obtained by upstream exponential extrapolation from the total experimental u' for $x > 600$ mm and equations (3.1). An inadequately described perturbation theory of Aizin (1974) and Aizin & Maksimov (1978) seems to invoke feedback. With many approximations the theory leads to an explicit expression for k_{13}, which is linear in $H(\exp \mathrm{i}k_{\mathrm{TSr}}l - 1)$, where l is the width of the strip, and is further dependent on the characteristics of the Orr–Sommerfeld operator and its adjoint. Total u' developments akin to that in our figure 1 were obtained for eleven distinct conditions; the corresponding coefficients k_{13} were extracted and compared with the formula in their table 1. The highest coefficient, 0.04, occurred for the largest H_3, 0.0345 mm, of our figure 1, and was within 1.3% of the theoretical value. Figure 1 indeed shows that an irradiated protuberance of miniscule height is effective in generating TS waves even though the coefficient is very small.

Discrepancies between experiment and theory exceeded 12% in five cases, two of which call for discussion. First, a non-zero coefficient k_{13} of 0.0064 was inferred from data for the polished plate without any artificial roughness. The authors decided that there must be an effective roughness at the aforementioned 'technological junction' at $x = 0.565$ m. From the theoretical linearity in H, corroborated well enough by the results for H_1, H_2 and H_3 in their figure 4, they assigned an effective H of 0.007–0.009 mm to the juncture. They did not undertake any more difficult measurements to verify this assessment on the bulky flat plate. Theoretical support for great 'scattering power' of small changes in local wall curvature comes from Goldstein's 1985 triple-deck approach to the problem. An implication of Goldstein's theory is that measurable local *mean* pressure gradients in x must be present to sustain the scattering capability. Whatever the exact cause of the 'effective roughness', the corresponding u'_{TS} growth is documented past Re_{δ^*} of 2200 in their figure 4, substantially downstream from the inferred initiation at Re_{δ^*} of 1550.

The second discrepancy of concern occurs relative to the dependence of k_{13} on the width of the strips l. Only two runs with l different from $l_1 = 12$ mm $= 0.24\lambda_{\mathrm{TS}}$ were made, namely for $l_2 = 0.5\lambda_{\mathrm{TS}}$ and $l_3 = \lambda_{\mathrm{TS}}$. The coefficient k_{13} for l_2 was 1.39 times larger than for l_1, in good agreement with theory. However, for l_3 the coefficient was 0.006 instead of zero. In the terminology of §4.3, substantial negative interference apparently takes place between Δu_{TS} increments initiated near the leading and

trailing edges of the mylar strips. The authors again attribute the non-zero contribution to the 'technological juncture' which 'inevitably creates a step on the surface of the strip' and cite the closeness of the two coefficients 0.0064 and 0.006 as supporting evidence. They also report that comparison with theory was made impossible when the 12 mm strip was moved downstream to $x = 1.127$ m (where $Re_{\delta^*} = 2200$) and the frequency raised above 100 Hz because 'the registered response was largely determined by the u'_{TS} contribution generated at the upstream juncture'. This documents again one major difficulty in receptivity experiments; the slowly developing impact of weak but effective sources is often camouflaged over long distances by other superposed signals and noise so that exact causes are hard to trace. Clearly, students of receptivity should be aware of such lessons from the experiments of Aizin & Polyakov as well as of their specific findings and interpretations.

REFERENCES

AIZIN, L. B. 1974 On the stability of weakly nonuniform states with small perturbations of white noise. *Prikl. Mat. Mekh.* **38**, No. 6 (in Russian).

AIZIN, L. B. & MAKSIMOV, V. P. 1978 On the stability of flow of weakly compressible gas in a pipe with model roughness. *Prikl. Mat. Mekh.* **42**, 650–655.

AIZIN, L. B. & POLYAKOV, N. F. 1979 Acoustic generation of Tollmien–Schlichting waves over local unevenness of surfaces immersed in streams. Preprint 17, Akad. Nauk, USSR, Siberian Div., Inst. Theor. & Applied Mech., Novosibirsk (in Russian).

BAR SEVER, A. 1984 Boundary layer transition over rough surfaces. MS thesis, Illinois Institute of Technology, Chicago, IL 60616.

BECHERT, D. W. 1982 Excited waves in shear layers. *DFVLR Rep.* FB 82-83. Inst. Exper. Fluid Mechanics, Göttingen, condensed in *AIAA Paper* 83-0724.

CORKE, T. C., BAR SEVER, A. & MORKOVIN, M. V. 1986 Experiments on transition enhancement by distributed roughness. *Phys. Fluids* (to appear).

DOVGAL, A. V., KACHANOV, YU. S., KOZLOV, V. V., LEVCHENKO, V. YA. & MAKSIMOV, V. P. 1979 Origin of perturbations in boundary layers. *Development of Perturbations in Boundary Layers*, Inst. Theor. & Applied Mech., Siberian Div. Akad. Nauk, USSR, pp. 4–22, Novosibirsk (in Russian). (Transl. in *NASA TM*-77986, 1986.)

DOVGAL, A. V. & KOZLOV, V. V. 1981*a* Generation of Tollmien–Schlichting waves by sound on blunt-nosed bodies. Preprint No. 21-81, Akad. Nauk, USSR, Siberian Div., Inst. Theor. & Applied Mech., Novosibirsk (in Russian).

DOVGAL, A. V. & KOZLOV, V. V. 1981*b* Influence of acoustic perturbations on the flow structure in boundary layers in adverse pressure gradients. Preprint 8-81, Akad. Nauk, USSR, Siberian Div., Inst. Theor. & Applied Mech., Novosibirsk (in Russian).

DOVGAL, A. V., KOZLOV, V. V. & LEVCHENKO, V. YA. 1980 Experimental investigation of reactions of a boundary layer to periodic external perturbations. *Izv. Akad. Nauk. SSSR. Mekh. Zhid. i Gaza* **4**, 155–159. (Transl. *Fluid Dyn.* 1981, 602–606.)

FASEL, H. 1976 Investigation of the stability of boundary layers by a finite difference model of the Navier–Stokes equations. *J. Fluid Mech.* **62**, 249–261.

GASTER, M. 1975 A theoretical model of a wave packet in the boundary layer on a flat plate. *Proc. R. Soc. Lond.* A **347**, 271–289.

GASTER, M. 1977 Series representation of the eigenvalues of the Orr–Sommerfeld equation. Paper 2 of *Laminar–Turbulent Transition*, *AGARD Conf. Proc.* 224.

GASTER, M. & GRANT, I. 1975 An experimental investigation of the formation and development of a wave packet in a laminar boundary layer. *Proc. R. Soc. Lond.* A **347**, 253–269.

GEDNEY, CH. J. 1983 The cancellation of a sound-excited Tollmien–Schlichting wave with plate vibrations. *Phys. Fluids* **26**, 1158–1160.

GINEVSKII, A. S., VLASOV, E. V. & KOLESNIKOV, A. V. 1978 *Aeroacoustic Interactions*. Moscow: Mashinostroenie.

GOLDSTEIN, M. E. 1983 The evolution of Tollmien–Schlichting waves near a leading edge. *J. Fluid Mech.* **127**, 59–81.

GOLDSTEIN, M. E. 1985 Scattering of acoustic waves into Tollmien–Schlichting waves by small streamwise variations in surface geometry. *J. Fluid Mech.* **154**, 509–529.

GOLDSTEIN, M. E. 1986 *Proc. ICASE/NASA 1985 Workshop on Stability of Time Dependent and Spacially Varying Flows.* Springer (to be published).

GOLDSTEIN, M. E., SOCKOL, P. M. & SANZ, J. 1983 Evolution of Tollmien–Schlichting waves near a leading edge. Part 2. Numerical determination of amplitudes. *J. Fluid Mech.* **129**, 443–453.

HAMA, F. R., WILLIAMS, D. R. & FASEL, H. 1980 Flow field and energy balance according to spatial linear stability theory of the Blasius boundary layer. In *Proc. IUTAM Symp. on Laminar–Turbulent Transition* (ed. R. Eppler & H. Fasel), pp. 73–85. Springer.

KACHANOV, YU. S., KOZLOV, V. V. & LEVCHENKO, V. YA. 1975 Generation and development of small disturbances in laminar boundary layers under the action of acoustic fields. *Akad. Nauk, USSR. Seria Tekhn. Nauk, Novosibirsk*, **13**, 18–26 (in Russian).

KACHANOV, YU, S., KOZLOV, V. V. & LEVCHENKO, V. YA. 1978 Origin of Tollmien–Schlichting waves in boundary layers under the influence of external disturbances. *Izv. Akad. Nauk. SSSR. Mekh. Zhid. i Gaza*, **5**, 85–94 (in Russian). (Transl. *Fluid Dyn.*, 1979, 704–11.)

KACHANOV, YU. S., KOZLOV, V. V. & LEVCHENKO, V. YA. 1982 *Initiation of Turbulence in Boundary Layers.* Novosibirsk: Nauka Publ. Siberian Div.

KACHANOV, YU. S., KOZLOV, V. V., LEVCHENKO, V. YA. & MAKSIMOV, V. P. 1979 Transformation of external disturbances into the boundary layer waves. In *Proc. Sixth Intl Conf. on Numerical Methods in Fluid Dynamics*, pp. 299–307. Springer.

KEGELMAN, J. 1982 Experimental studies of boundary-layer transition on a spinning and non-spinning axisymmetric body. Ph.D. thesis, Notre Dame University IN 46556, USA.

KEGELMAN, J. T. & MUELLER, T. J. 1986 Experimental studies of spontaneous and forced transition on an axisymmetric body. *AIAA J.* **24**, 397–403.

KENDALL, J. M. 1984 Experiments on the generation of Tollmien–Schlichting waves in a flat plate boundary layer by weak free-stream turbulence. *AIAA Paper No.* 84-0011.

KNAPP, C. F. & ROACHE, P. J. 1968 A combined visual and hot-wire anemometer investigation of boundary layer transition. *AIAA J.* **6**, 29–36.

KOZLOV, V. V. (ed.) 1985 *Proc. 2nd Symp. on Laminar–Turbulent Transition*, pp. 233–248, 283–320. Springer.

LEEHEY, P. 1980 The influence of environment in laminar boundary layer control. In *Proc. 2nd Symp. on Viscous Drag Reduction* (ed. G. R. Hough), *AIAA Prog. in Astro & Aero.*, vol. 72.

LEEHEY, P. & SHAPIRO, P. 1980 Leading-edge effect in laminary boundary layer excitation by sound. In *Proc. IUTAM Symp. on Laminar–Turbulent Transition* (ed. R. Eppler & H. Fasel), pp. 321–331. Springer.

LEMCKE, L., NAYSMITH, A., PICKEN, J. & THOMANN, H. 1970 Comparison of heat transfer measurements in free flight and in wind tunnel at $M = 7$ at similar Reynolds numbers and temperature ratios. In *Proc. 7th Congress Intl Council Aeron. Sci., Rome.*

LIEPMANN, H. W., BROWN, G. L. & NOSENCHUCK, D. M. 1982 Control of laminar-instability waves using a new technique. *J. Fluid Mech.* **118**, 187–200.

LIGHTHILL, M. J. 1963 Boundary layer theory. In *Laminar Boundary Layers* (ed. L. Rosenhead). Oxford University Press.

LIN, C. C. 1955 *The Theory of Hydrodynamic Stability.* Cambridge University Press.

LOEHRKE, R. I., MORKOVIN, M. V. & FEJER, A. A. 1975 Review: Transition in nonreversing oscillating boundary layers. *Trans. ASME* I: *J. Fluids Engng* **97**, 534–549.

MAKSIMOV, V. P. 1979 Genesis of Tollmien–Schlichting waves in oscillating boundary layers (in Russian). In *Development of Perturbations in Boundary Layers* (ed. V. Ya. Levchenko), pp. 68–75. Inst. Theor. & Applied Mech., Siberian Div. Akad. Nauk USSR. Novosibirsk.

MORKOVIN, M. V. 1978 Instability, transition to turbulence and predictability. *AGARDograph* 236.

MORKOVIN, M. V. & PARANJAPE, S. V. 1971 On acoustic excitation of shear layers. *Zeit. Flugwiss.* **19**, 328–335.

MORSE, P. M. & INGARD, K. U. 1968 *Theoretical Acoustics.* McGraw-Hill.

MUNGUR, C. J. 1977 On the sensitivity of shear layers to sound. *AIAA Paper No.* 77-1369.

MURDOCK, J. W. 1980 The generation of Tollmien–Schlichting wave by a sound wave. *Proc. R. Soc. Lond.* A **372**, 1517.

POLYAKOV, N. F. 1979 Laminar boundary layer in "natural" transition to turbulence. In *Development of Perturbations in Boundary Layers* (ed. V. Ya. Levchenko), pp. 23–67. Inst. Theor. & Applied Mech., Siberian Div. Akad. Nauk USSR, Novosibirsk (in Russian).

POLYAKOV, N. F., DOMARATSKII, A. N. & SKURLATOV, A. I. 1976 On the interaction of acoustic fields with incompressible laminar boundary layers. *Izv. Sib. Otd. Akad. Nauk. USSR Seria Tekhn. Nauk, Novosibirsk* **13**, 19–27 (in Russian).

RESHOTKO, E. 1976 Boundary stability and transition. *Ann. Rev. Fluid Mech.* **8**, 311–350.

RESHOTKO, E. 1984 Environment and receptivity. In *Special Course on Stability and Transition of Laminar Flow* (ed. R. Michel), section 4. *AGARD Rep.* 709.

SALWEN, H. & GROSCH, CH. E. 1981 The continuous spectrum of the Orr–Sommerfeld equation. Part 2. Eigenfunction expansions. *J. Fluid Mech.* **104**, 445–465.

SCHUBAUER, G. B. & SKRAMSTAD, H. K. 1948 Laminary boundary-layer oscillations and transition on a flat plate. *NACA Tech. Rep.* 909.

SHAPIRO, P. J. 1977 The influence of sound upon laminar boundary layer instability. *MIT Acoustics and Vibration Lab. Rep.* 83458-83560-1.

SPANGLER, I. G. & WELLS, C. S. 1968 Effects of free-stream disturbances on boundary-layer transition. *AIAA J.* **6**, 543–545.

TAM, CH. K. W. 1981 The excitation of Tollmien–Schlichting waves in low subsonic boundary layers by free-stream sound waves. *J. Fluid Mech.* **109**, 483–501.

THOMAS, A. S. W. 1984 Control of boundary-layer transition using a wave-superposition principle. *J. Fluid Mech.* **137**, 233–250.

VLASOV, E. V., GINEVSKII, A. S. & KARAVOSOV, R. K. 1977 Reaction of an unstable laminar boundary layer to acoustic excitation. In *Turbulent Flows*, pp. 90–96. Moscow: Nauka (in Russian).

WAZZAN, A. R., OKAMURA, T. T. & SMITH, A. M. O. 1969 Stability characteristics of the Falkner–Skan profiles. Enclosure in *A Portfolio of Stability Characteristics of Incompressible Boundary Layers* (by H. J. Obremski, M. V. Morkovin & M. Landahl). *AGARDograph no.* 134.